Editors' Suggestion

Relativistic imprints on dispersion measure space distortions

Shohei Saga[1,2,3,*] and David Alonso[4]

[1]Institute for Advanced Research, Nagoya University, Furo-cho Chikusa-ku, Nagoya 464-8601, Japan
[2]Kobayashi-Maskawa Institute for the Origin of Particles and the Universe, Nagoya University, Chikusa-ku, Nagoya, 464-8602, Japan
[3]Sorbonne Université, CNRS, UMR7095, Institut d'Astrophysique de Paris, 98bis boulevard Arago, F-75014 Paris, France
[4]Department of Physics, University of Oxford, Denys Wilkinson Building, Keble Road, Oxford OX1 3RH, United Kingdom

(Received 12 April 2024; accepted 16 September 2024; published 25 September 2024)

We investigate the three-dimensional clustering of sources emitting electromagnetic pulses traveling through cold electron plasma, whose radial distance is inferred from their dispersion measure. As a distance indicator, dispersion measure is systematically affected by inhomogeneities in the electron density along the line of sight and special and general relativistic effects, similar to the case of redshift surveys. We present analytic expressions for the correlation function of fast radio bursts (FRBs) and for the galaxy-FRB cross-correlation function, in the presence of these *dispersion measure-space distortions*. We find that the even multipoles of these correlations are primarily dominated by nonlocal contributions (e.g., the electron density fluctuations integrated along the line of sight), while the dipole also receives a significant contribution from the Doppler effect, one of the major relativistic effects. A large number of FRBs, $\mathcal{O}(10^5\text{–}10^6)$, expected to be observed in the Square Kilometre Array, would be enough to measure the even multipoles at very high significance, $\mathrm{S/N} \approx 100$, and perhaps to make a first detection of the dipole ($\mathrm{S/N} \approx 10$) in the FRB correlation function and FRB-galaxy cross correlation function. This measurement could open a new window to study and test cosmological models.

DOI: 10.1103/PhysRevD.110.063556

I. INTRODUCTION

Fast radio bursts (FRBs) are radio transients with millisecond duration first detected by Ref. [1]. The radio pulses emitted from FRBs travel through the cold ionized intergalactic medium, and their arrival time receives a frequency dependence that depends on the column density of free electrons through the so-called dispersion measure (DM, see Ref. [2] for details). Recent observations of FRBs have found DMs far larger ($\gtrsim 500\ \mathrm{pc\,cm^{-3}}$) than would be expected for any single source ($\sim 100\ \mathrm{pc\,cm^{-3}}$), suggesting that they reside in extragalactic sources. This is supported by the redshifts measured for small samples of localized FRBs, although their specific origin is still under debate (see Refs. [3–7] and also Refs. [8–10] for recent reviews). Future surveys such as UTMOST,[1] HIRAX,[2] and Square Kilometre Array (SKA)[3] will detect more than thousands of FRBs per year [11–15] and provide large FRB catalogs across cosmological scales. It is therefore interesting to study the possibility of using FRBs as a new cosmological probe, complementary to the cosmic microwave background and galaxy surveys.

Since the DM is given by the column density of free electrons along the pulse's path, DM measurements may contain important information about the baryonic content of the intergalactic medium, such as, the reionization history [16–23], the gas mass fraction in the cosmic web [24–27], baryonic effects [28,29], and even important clues about the missing baryon problem [30–34]. As FRBs may originate at high redshifts, they may also constitute a tool to obtain constraints on cosmological parameters, such as the equation of state of dark energy [35–40], the baryon density [41–45], or the Hubble parameter [46–51]. FRB data may also be used to test the equivalence principle [52–55], and primordial non-Gaussianity [56].

As a cosmological distance measure in the absence of redshift information, DM is called *standard ping* [57,58] and enables us to construct three-dimensional maps of FRB catalogs. However, the DM receives a significant stochastic contribution from the propagation of the FRB pulse through the inhomogeneous universe and is therefore far from a perfect distance proxy. The corresponding DM-based 3D map of the large-scale structure therefore

*Contact author: shohei.saga@yukawa.kyoto-u.ac.jp
[1]https://astronomy.swin.edu.au/research/utmost/.
[2]https://hirax.ukzn.ac.za/.
[3]https://www.skao.int/.

appears to be distorted in the radial direction, the so-called *dispersion measure space distortions*. The primary contributor to the distortions is the inhomogeneous distribution of free electrons [32,36,57,58]. On top of this contribution, Ref. [59] has shown that special and general relativistic effects also induce additional distortions (see also Ref. [60] for the Shapiro time delay effect of dark matter substructure on the variance of the DM). Restricting ourselves to two-dimensional statistics, such as the angular power spectrum of projected DM observations, the relativistic effects remain a minor contributor that is likely unobservable.

The impact of relativistic effects and redshift-space distortions (RSDs) in galaxy redshift surveys has been investigated [61–64]. The characteristic signal of relativistic effects in RSDs is the asymmetric distortions along the line-of-sight direction [65–69], suggesting that investigating the galaxy clustering in the three-dimensional space is crucial to target relativistic effects.

Motivated by the above, in this paper, we investigate the anisotropy of the three-dimensional clustering in DM space, including both the inhomogeneous free electron distribution and relativistic effects based on Refs. [57–59]. Analogous to RSDs, relativistic effects produce an asymmetric clustering with respect to the line-of-sight direction. This asymmetry is characterized by a dipole in the multipole expansion of the correlation function. In this paper, we investigate the behavior of the dipole anisotropy as well as the even multipole anisotropy. The former captures the impact of the relativistic effects, while the latter captures the impact of the inhomogeneous distribution of free electrons, both of which are complementary and therefore important observables for testing cosmological models and gravity theories. Based on the derived analytical expression for the multipoles, we also discuss the future detectability in an SKA-like survey for the multipoles of the FRBs cross-power spectra and in the galaxy-FRB cross-power spectra. Our investigation mainly focuses on the FRBs but applies to other standard pings (i.e., other bright radio transients having short timescales).

This paper is organized as follows. In Sec. II, we briefly introduce DM-based observations in a perturbed Friedmann-Lemaître-Robertson-Walker (FLRW) universe and present the analytical expression of the density field in DM space, following Ref. [59]. In Sec. III and Sec. IV, we consider the cross-correlation between FRBs with different biases and the cross-correlation between galaxies and FRBs, respectively. In these sections, we present the analytical expression of the correlation function in DM space and numerically investigate their behavior. In Sec. V, we forecast the expected signal-to-noise ratio for these measurements assuming SKA-like survey specifications. We conclude and summarize our results in Sec. VI. We adopt the distant-observer limit throughout the analysis but discuss the wide-angle correction in Appendix A. We also investigate the correction from the nonlinear matter power spectrum to the dipole signal in Appendix B. We discuss the impact from the host galaxies on the correlation function in Appendix C. Throughout this paper, we apply the Einstein summation convention for repeated Greek and Latin indices, running from 0 to 3 and from 1 to 3, respectively. We work in units $c = \hbar = 1$.

II. THREE-DIMENSIONAL CLUSTERING IN DM SPACE

As the DM of electromagnetic pulses depends on the cumulative amount of plasma along the trajectory, we can regard it as a radial distance proxy and reconstruct the three-dimensional clustering of pulse emitters. However, the DM is not a perfect proxy for a radial distance because of inhomogeneities in the electron density (e.g., Refs. [32,36,57,58]). In addition to the electron density inhomogeneities, special and general relativistic effects have an impact on the trajectories and energies of the emitted photons, and thus, the DM is further modulated. Hence, the observed DM-based clustering pattern appears to be distorted [59]. In this section, we briefly review the observed density field in DM space following in the footsteps of Ref. [59]. Throughout our analysis, we simply assume that DM is directly related to the number density of cold electron plasma in the intergalactic medium and ignore the local contributions (i.e., free electrons of host galaxies and in the Milky Way). This systematic would introduce suppression of the signal at small radial scales if the local contribution does not correlate to the cosmological signal in the intergalactic medium [70]. We discuss the impact from the free electrons of host galaxies on the correlation functions in Appendix C.

The DM of pulses is given by [59]

$$\mathcal{D} = \int_{\lambda_e}^{\lambda_o} \mathrm{d}\lambda \left(n_e \frac{k^\mu u_{e,\mu}}{1+z} \right) \bigg|_\lambda . \qquad (1)$$

Here, we define the redshift z, the four-momentum of the massless pulse $k^\mu = \mathrm{d}x^\mu/\mathrm{d}\lambda$, with λ being an affine parameter, the affine parameter at the observer λ_o, the affine parameter at the source λ_e, the four-velocity of the source $u_{e,\mu}$, and the electron number density n_e. The subscript λ indicates that the integrand is evaluated along the trajectory of the pulse, corresponding to a null geodesic.

Consider the perturbed FLRW metric,

$$\mathrm{d}s^2 = a^2\left[(1+2\psi)\mathrm{d}\eta^2 - (1-2\phi)\mathrm{d}x^2\right], \qquad (2)$$

where the quantities a and η are the scale factor and the conformal time, respectively. Here, we consider only the scalar perturbations, ψ and ϕ. Up to the linear order in the perturbed variables, Eq. (1) is given by [59]

$$\mathcal{D}(\eta,\hat{\boldsymbol{n}}) = \int_\eta^{\eta_0} \mathrm{d}\eta'\, a^2(\eta')\bar{n}_\mathrm{e}(\eta') \times \Bigg[1+\delta_\mathrm{e}(\eta',\chi'\hat{\boldsymbol{n}}) + 2\psi(\eta',\chi'\hat{\boldsymbol{n}}) + \int_{\eta'}^{\eta_0}\mathrm{d}\eta''(\dot{\psi}(\eta'',\chi''\hat{\boldsymbol{n}}) + \dot{\phi}(\eta'',\chi''\hat{\boldsymbol{n}}))\Bigg], \quad (3)$$

where the quantities η_0 and $\hat{\boldsymbol{n}}$ are, respectively, the conformal time at the present and the unit vector $\hat{\boldsymbol{n}} = \boldsymbol{x}/|\boldsymbol{x}| = \boldsymbol{x}/\chi$ with $\chi = \eta_0 - \eta$ being the radial comoving distance. A dot denotes a derivative with respect to the conformal time. Here, we decomposed the electron density into background and perturbation $n_\mathrm{e} = \bar{n}_\mathrm{e}(1+\delta_\mathrm{e})$. In deriving Eq. (3), we solved the geodesic equation in the perturbed FLRW metric (see, e.g., Refs. [63,64] and also Appendix A in Ref. [59] in details). We note that ignoring the perturbations in Eq. (3), we recover the background expression of the DM,

$$\bar{\mathcal{D}}(z) = \int_0^z \mathrm{d}z' \frac{(1+z')}{H(z')} a^3(z')\bar{n}_\mathrm{e}(z'). \quad (4)$$

Reference [59] derived an analytical expression for the number density of observed sources in an observer's solid angle $\mathrm{d}\Omega_o$ and DM interval $\mathrm{d}\mathcal{D}$, in a manner analogous to the galaxy redshift survey [63,64]. We refer the readers to Ref. [59] for the details of the derivation and present only the final result. Assuming $\phi = \psi$, the expression of the fluctuation of the number density in DM space $\delta_\mathrm{X}^{(\mathcal{D})}$ for the species X is given by

$$\delta_\mathrm{X}^{(\mathcal{D})} = \delta_\mathrm{X} - \delta_\mathrm{e} + \boldsymbol{v}\cdot\hat{\boldsymbol{n}} - 2\hat{\nabla}^2\int_0^\chi \mathrm{d}\chi' \frac{\chi-\chi'}{\chi\chi'}\phi + \mathcal{A}_\mathrm{X}(\chi)\frac{\mathcal{H}}{a^2\bar{n}_\mathrm{e}}\int_\eta^{\eta_0}\mathrm{d}\eta'\, a^2\bar{n}_\mathrm{e}\left(\delta_\mathrm{e} + 2\phi + 2\int_{\eta'}^{\eta_0}\mathrm{d}\eta''\dot{\phi}\right) - 3\phi - 2\int_\eta^{\eta_0}\mathrm{d}\eta'\,\dot{\phi} + \frac{4}{\chi}\int_\eta^{\eta_0}\mathrm{d}\eta'\phi, \quad (5)$$

where the quantities δ_X, $\boldsymbol{v}$, and $\mathcal{H} = \dot{a}/a$ are the density fluctuation of the source number density for the species X, the source velocity, and the reduced Hubble parameter, respectively. The operators $\hat{\boldsymbol{\nabla}}$ and $\hat{\nabla}^2$ are the angular gradient and angular Laplacian, respectively. These operators satisfy the following relations: $\hat{\nabla}_i\hat{n}_j = -\hat{n}_i\hat{n}_j + \delta_{ij}$ and $\hat{\nabla}^2\hat{\boldsymbol{n}} = -2\hat{\boldsymbol{n}}$. The quantity $\mathcal{A}_\mathrm{X}(\chi)$ defined in Eq. (5) is explicitly given by

$$\mathcal{A}_\mathrm{X}(\chi) = 1 + f_\mathrm{X} - f_\mathrm{e} - \frac{2}{\mathcal{H}\chi}, \quad (6)$$

with $f_i \equiv \mathrm{d}\ln(a^3\bar{n}_i)/\mathrm{d}\ln a$ being the evolution bias for the species i.

Equation (5) is our starting expression of the DM space density. The third and fourth terms on the right-hand side are, respectively, a velocity term arising from the distortions of the observed comoving volume and weak lensing term. Here, we simply ignored the magnification bias, which changes the prefactor of the weak lensing term. The second and third lines, respectively, correspond to the nonlocal density term arising from the light cone integral of the DM and the other relativistic terms including the Sachs-Wolfe, Shapiro time delay, and integrated Sachs-Wolfe effects.

Importantly, the contributions proportional to $\mathcal{O}((\mathcal{H}/k)^2)$ are suppressed with respect to the density and weak lensing terms. Ignoring these subdominant contributions, Eq. (5) becomes

$$\delta_\mathrm{X}^{(\mathcal{D})}(\eta,\boldsymbol{x}) = \delta_\mathrm{X}^\mathrm{l}(\eta,\boldsymbol{x}) + \delta_\mathrm{X}^\mathrm{v}(\eta,\boldsymbol{x}) + \delta_\mathrm{X}^\mathrm{lc}(\eta,\boldsymbol{x}) + \delta_\mathrm{X}^\kappa(\eta,\boldsymbol{x}), \quad (7)$$

where we define

$$\delta_\mathrm{X}^\mathrm{l}(\eta,\boldsymbol{x}) = (b_\mathrm{X} - b_\mathrm{e})\delta_\mathrm{L}(\eta,\boldsymbol{x}), \quad (8)$$

$$\delta_\mathrm{X}^\mathrm{v}(\eta,\boldsymbol{x}) = \boldsymbol{v}(\eta,\boldsymbol{x})\cdot\hat{\boldsymbol{n}}, \quad (9)$$

$$\delta_\mathrm{X}^\mathrm{lc}(\eta,\boldsymbol{x}) = \mathcal{A}_\mathrm{X}(\chi)b_\mathrm{e}\frac{\mathcal{H}}{a^2\bar{n}_\mathrm{e}}\int_\eta^{\eta_0}\mathrm{d}\eta'\, a^2\bar{n}_\mathrm{e}\delta_\mathrm{L}(\eta',\chi'\hat{\boldsymbol{n}}), \quad (10)$$

$$\delta_\mathrm{X}^\kappa(\eta,\boldsymbol{x}) = -2\hat{\nabla}^2\int_0^\chi \mathrm{d}\chi'\frac{\chi-\chi'}{\chi\chi'}\phi(\eta',\chi'\hat{\boldsymbol{n}}). \quad (11)$$

We assume a linear bias relation for the source and electron densities, in which each density field is related to the linear density field δ_L via $\delta_\mathrm{X} = b_\mathrm{X}\delta_\mathrm{L}$ and $\delta_\mathrm{e} = b_\mathrm{e}\delta_\mathrm{L}$. The first to fourth terms on the right-hand side in Eq. (7) correspond to the local density, local velocity, nonlocal density integrated along the unperturbed past light cone, and lensing contributions, respectively. We evaluate the integrands of the nonlocal terms in Eqs. (10) and (11) along the null geodesic, with $\chi' = \eta_0 - \eta'$.

Moving into Fourier space, Eqs. (8)–(11) become

$$\delta_\mathrm{X}^\mathrm{l}(\eta,\boldsymbol{x}) = (b_\mathrm{X} - b_\mathrm{e})\int\frac{\mathrm{d}^3\boldsymbol{k}}{(2\pi)^3}e^{i\boldsymbol{k}\cdot\boldsymbol{x}}\delta_\mathrm{L}(\eta,\boldsymbol{k}), \quad (12)$$

$$\delta_\mathrm{X}^\mathrm{v}(\eta,\boldsymbol{x}) = \int\frac{\mathrm{d}^3\boldsymbol{k}}{(2\pi)^3}e^{i\boldsymbol{k}\cdot\boldsymbol{x}}(i\hat{\boldsymbol{k}}\cdot\hat{\boldsymbol{n}})\frac{\mathcal{H}f}{k}\delta_\mathrm{L}(\eta,\boldsymbol{k}), \quad (13)$$

$$\delta_\mathrm{X}^\mathrm{lc}(\eta,\boldsymbol{x}) = \mathcal{A}_\mathrm{X}(\chi)b_\mathrm{e}\frac{\mathcal{H}}{a^2\bar{n}_\mathrm{e}}\int_0^\chi\mathrm{d}\chi'\, a^2(\eta')\bar{n}_\mathrm{e}(\eta') \times\int\frac{\mathrm{d}^3\boldsymbol{k}}{(2\pi)^3}e^{i\boldsymbol{k}\cdot(\chi'\hat{\boldsymbol{n}})}\delta_\mathrm{L}(\eta',\boldsymbol{k}), \quad (14)$$

$$\delta^{\kappa}_{\rm X}(\eta,\boldsymbol{x}) = 3\Omega_{\rm m0}\mathcal{H}_0^2\int_0^{\chi}{\rm d}\chi'\frac{\chi-\chi'}{\chi\chi'}\int\frac{{\rm d}^3\boldsymbol{k}}{(2\pi)^3}e^{i\boldsymbol{k}\cdot(\chi'\hat{\boldsymbol{n}})} \times\frac{-\chi'^2k_\perp^2-2i\chi'k_\parallel}{a(\eta')k^2}\delta_{\rm L}(\eta',\boldsymbol{k}), \tag{15}$$

where the quantities $\Omega_{\rm m0}$, $\mathcal{H}_0$, and f are the matter density parameter, reduced Hubble parameter at the present time, and the linear growth rate. f is defined by $f\equiv {\rm d}\ln D_+/{\rm d}\ln a$ with D_+ the linear growth factor. We assume self-similar growth in the linear regime, such that $\delta_{\rm L}(\eta,\boldsymbol{k}) = D_+(\eta)\delta_{\rm L}(\eta_0,\boldsymbol{k})$. We define the longitudinal and transverse components of the wave vector as $k_\parallel = \boldsymbol{k}\cdot\hat{\boldsymbol{n}}$ and $k_{\perp,i} = (\delta_{ia}-\hat{n}_i\hat{n}_a)k_a$, respectively.

In deriving the expressions above, we assume the following transfer functions:

$$\phi(\eta,\boldsymbol{k}) = -\frac{3\Omega_{\rm m0}\mathcal{H}_0^2}{2ak^2}\delta_{\rm L}(\eta,\boldsymbol{k}), \tag{16}$$

$$\boldsymbol{v}(\eta,\boldsymbol{k}) = i\hat{\boldsymbol{k}}\frac{\mathcal{H}f}{k}\delta_{\rm L}(\eta,\boldsymbol{k}). \tag{17}$$

Equation (7) together with Eqs. (12)–(15) presents the relation between the observed density fluctuation in DM space and real space density field. These expressions are key ingredients to compute the two-point statistics of the clustering of FRBs in DM space.

III. FRB CORRELATION FUNCTION

In this section, starting from the expression for the density field in DM space presented above, we investigate the FRB correlation function in DM space. We consider the general situation where we can observe two populations of FRBs, X and Y, and we study the correlation of their overdensities measured at DM-space positions $\boldsymbol{x}_1$ and $\boldsymbol{x}_2$, respectively [which we denote $\delta^{(\mathcal{D})}_{\rm X}(\boldsymbol{x}_1)$ and $\delta^{(\mathcal{D})}_{\rm Y}(\boldsymbol{x}_2)$]. Separating FRBs into different populations is possible, for example, if their host galaxies can be identified and split by brightness or color, leading to populations with different effective biases (e.g., Ref. [71]). The exact procedure to separate these two populations with sufficiently different biases will be subject to statistic and systematic uncertainties. Here, we will simply assume that such a split is possible and make predictions for the resulting cross-correlation function. Later on, we will present the cross-correlation between galaxies and FRBs, which would not be significantly affected by these uncertainties.

We compute the cross-correlation,

$$\xi_{\rm XY}(\boldsymbol{x}_1,\boldsymbol{x}_2) = \left\langle\delta^{(\mathcal{D})}_{\rm X}(\boldsymbol{x}_1)\delta^{(\mathcal{D})}_{\rm Y}(\boldsymbol{x}_2)\right\rangle, \tag{18}$$

with $\langle\cdots\rangle$ denoting the ensemble average. We omit all time dependence for brevity. In computing the correlation function, we assume the distant-observer limit, i.e., $\hat{\boldsymbol{n}}_1 = \hat{\boldsymbol{n}}_2 = \hat{z}$ with $\hat{z}$ being a fixed line-of-sight vector. Under the distant-observer limit, the correlation function is given as a function of the separation $s=|\boldsymbol{s}|=|\boldsymbol{x}_2-\boldsymbol{x}_1|$ and the directional cosine μ between $\hat{z}$ and $\hat{\boldsymbol{s}}$. For the nonlocal terms, we use the Limber approximation [72] (see Refs. [62,68,73,74]). In Appendix A, we discuss the wide-angle correction beyond the distant-observer limit, which is, however, negligibly small.

Substituting Eq. (7) into Eq. (18), we derive the analytical expression for the correlation function. We split the nonvanishing contributions into eight pieces,

$$\xi_{\rm XY} = \left(\xi^{\rm l\times l}_{\rm XY}+\xi^{\rm l\times v}_{\rm XY}+\xi^{\rm v\times v}_{\rm XY}\right)+\left(\xi^{\rm lc\times lc}_{\rm XY}+\xi^{\rm lc\times\kappa}_{\rm XY}+\xi^{\kappa\times\kappa}_{\rm XY}\right) +\left(\xi^{\rm l\times lc}_{\rm XY}+\xi^{\rm l\times\kappa}_{\rm XY}\right), \tag{19}$$

where we define

$$\xi^{\rm a\times b}_{\rm XY} = \begin{cases}\langle\delta^{\rm a}_{\rm X}(\boldsymbol{x}_1)\delta^{\rm b}_{\rm Y}(\boldsymbol{x}_2)\rangle & ({\rm a}={\rm b})\\ \langle\delta^{\rm a}_{\rm X}(\boldsymbol{x}_1)\delta^{\rm b}_{\rm Y}(\boldsymbol{x}_2)\rangle+({\rm a}\leftrightarrow{\rm b}) & ({\rm a}\neq{\rm b})\end{cases}. \tag{20}$$

The first, second, and third parentheses in the right-hand side of Eq. (19) stand for the pure local term arising from the local density and local velocity terms, the pure nonlocal term arising from the nonlocal density and weak lensing terms, and the cross-correlation between local and nonlocal terms, respectively. The cross-correlations between the local velocity and nonlocal terms vanish, i.e., $\langle\delta^{\rm v}_{\rm X}\delta^{\rm lc}_{\rm Y}\rangle = \langle\delta^{\rm v}_{\rm X}\delta^{\kappa}_{\rm Y}\rangle = 0$, because the parallel components to the line-of-sight direction do not contribute to the correlation function in the flat-sky, Limber approximation (see, e.g., Refs. [68,70,75,76]).

The explicit forms of the right-hand side of Eq. (19) are given by

$$\xi^{\rm l\times l}_{\rm XY} = (b_{\rm X}-b_{\rm e})(b_{\rm Y}-b_{\rm e})\Xi^{(0)}_0(\eta,s), \tag{21}$$

$$\xi^{\rm l\times v}_{\rm XY} = -(b_{\rm X}-b_{\rm Y})\mu(s\mathcal{H}f)\Xi^{(1)}_1(\eta,s), \tag{22}$$

$$\xi^{v\times v}_{\rm XY} = (s\mathcal{H}f)^2\left[\left(\frac{1}{3}-\mu^2\right)\Xi^{(2)}_2(\eta,s)+\frac{1}{3}\Xi^{(2)}_0(\eta,s)\right], \tag{23}$$

for the purely local contributions,

$$\xi^{\rm lc\times lc}_{\rm XY} = \mathcal{A}_{\rm X}(\chi)\mathcal{A}_{\rm Y}(\chi)\left(b_{\rm e}\frac{\mathcal{H}}{a^2\bar{n}_{\rm e}}\right)^2\int_0^{\chi}{\rm d}\chi' \times(a^2(\eta')\bar{n}_{\rm e}(\eta'))^2\mathcal{J}\left(\eta',\frac{\chi'}{\chi}s\sqrt{1-\mu^2}\right), \tag{24}$$

$$\xi^{\rm lc\times\kappa}_{\rm XY} = -(\mathcal{A}_{\rm X}(\chi)+\mathcal{A}_{\rm Y}(\chi))b_{\rm e}\frac{\mathcal{H}}{a^2\bar{n}_{\rm e}}\frac{3\Omega_{\rm m0}\mathcal{H}_0^2}{\chi}\int_0^{\chi}{\rm d}\chi' \times a(\eta')\bar{n}_{\rm e}(\eta')(\chi-\chi')\chi'\mathcal{J}\left(\eta',\frac{\chi'}{\chi}s\sqrt{1-\mu^2}\right), \tag{25}$$

$$\xi^{\kappa\times\kappa}_{\rm XY} = \left(\frac{3\Omega_{\rm m0}\mathcal{H}_0^2}{\chi}\right)^2 \int_0^{\chi} {\rm d}\chi' \times \left(\frac{(\chi-\chi')\chi'}{a(\eta')}\right)^2 \mathcal{J}\left(\eta', \frac{\chi'}{\chi} s\sqrt{1-\mu^2}\right), \tag{26}$$

for the purely nonlocal contributions, and

$$\xi^{\rm l\times lc}_{\rm XY} = (\Theta(\chi_2-\chi_1)(b_{\rm X}-b_{\rm e})\mathcal{A}_{\rm Y} + \Theta(\chi_1-\chi_2)(b_{\rm Y}-b_{\rm e})\mathcal{A}_{\rm X})b_{\rm e}\mathcal{H}\mathcal{J}\left(\eta, s\sqrt{1-\mu^2}\right), \tag{27}$$

$$\xi^{\rm l\times\kappa}_{\rm XY} = (-\Theta(\chi_2-\chi_1)(b_{\rm X}-b_{\rm e}) + \Theta(\chi_1-\chi_2)(b_{\rm Y}-b_{\rm e})) \times \frac{3\Omega_{\rm m0}\mathcal{H}_0^2}{a} s\mu\mathcal{J}\left(\eta, s\sqrt{1-\mu^2}\right), \tag{28}$$

for the cross-correlation between them. In the above, we define the following functions:

$$\Xi^{(n)}_\ell(\eta, s) = \int \frac{k^2{\rm d}k}{2\pi^2}\frac{j_\ell(ks)}{(ks)^n}P_{\rm L}(\eta, k), \tag{29}$$

$$\mathcal{J}(\eta, s) = \int \frac{{\rm d}k}{2\pi} kJ_0(ks)P_{\rm L}(\eta, k), \tag{30}$$

where the functions j_ℓ and J_0 are, respectively, the spherical Bessel function of order ℓ, and the Bessel function of the first kind of order zero. We define the linear matter power spectrum at the time η: $\langle\delta_{\rm L}(\eta,\boldsymbol{k})\delta_{\rm L}(\eta,\boldsymbol{k}')\rangle = (2\pi)^3\delta^3_{\rm D}(\boldsymbol{k}+\boldsymbol{k}')P_{\rm L}(\eta,k)$.

As a consequence of the DM-space distortions, the derived expressions depend on the directional cosine μ. As done in the standard analysis of galaxy clustering in redshift space, we quantify this anisotroy by using a multipole expansion of the correlation function, weighting with the Legendre polynomials $\mathcal{L}_\ell(\mu)$ with $\mu = \hat{\boldsymbol{s}}\cdot\hat{\boldsymbol{z}}$,

$$\xi_\ell(s) = \frac{2\ell+1}{2}\int_{-1}^{1}{\rm d}\mu\, \xi_{\rm XY}(s,\mu)\mathcal{L}_\ell(\mu). \tag{31}$$

In the local contributions (21)–(23), the velocity term induces the anisotropy in the correlation function. This induced anisotropy comes not from the standard Kaiser effect, seen in redshift space, but due to observed volume distortions (i.e., a pure relativistic effect). Interestingly, the cross-correlation between the local density and local velocity given in Eq. (22) exhibits the asymmetric clustering along the line-of-sight direction, i.e., contributes to a dipole ($\ell = 1$) anisotropy. This dipole contribution is nonzero only when we cross-correlate samples with different biases, due to the prefactor $b_{\rm X} - b_{\rm Y}$. This effect is also reproduced in the redshift-space clustering of galaxies (see, e.g., Refs. [65–69,77–83]). The cross-correlation between the local and nonlocal contributions (27)–(28) produces both even and odd multipoles, while the pure nonlocal contributions (24)–(26) produce only even multipoles because of their symmetric dependence on μ. From these analytical expressions, the local contributions (21)–(23) induce only anisotropies with $\ell \leq 2$, whereas the nonlocal contributions (24)–(28) contribute to arbitrarily high multipoles.

In Fig. 1, we numerically demonstrate the contributions to the first three multipoles, i.e., the monopole ($\ell = 0$), dipole ($\ell = 1$), and quadrupole ($\ell = 2$). In this plot, we model the background electron density as [59]

$$\bar{n}_{\rm e} = \frac{3H_0^2\Omega_{\rm b0}}{8\pi G m_{\rm p}}\frac{x_{\rm e}(z)(1+x_{\rm H}(z))}{2}a^{-3}, \tag{32}$$

where we use $x_{\rm H} = 0.75$ and $x_{\rm e} = 1$ for simplicity. Through Eq. (4) together with Eqs. (32), the background DM is a monotonic function of redshift z. Therefore, to facilitate the interpretation of our results, throughout the rest of this paper, we present results using redshift as a time indicator in the light cone.

We assume a mean bias given by the specifications of SKA2 HI galaxies given in Ref. [84],

$$b_{\rm SKA}(z) = c_4 \exp(c_5 z), \tag{33}$$

with $c_4 = 0.554$ and $c_5 = 0.783$. We note that there is no evidence that HI galaxies are the preferential hosts of FRBs, and we only use this parametrization in order to produce results assuming realistic galaxy bias values. We split the full FRB host population into two subsamples with different biases,

$$b_{\rm X}(z) = b_{\rm SKA}(z) + \Delta b/2, \tag{34}$$

$$b_{\rm Y}(z) = b_{\rm SKA}(z) - \Delta b/2. \tag{35}$$

We adopt an arbitrary bias difference $b_{\rm X} - b_{\rm Y} = \Delta b = 1$, noting again that our results, particularly in the case of the FRB-FRB correlations, depend on our ability to select such subsamples.

As shown in Fig. 1, we find that the even multipoles (top two panels) are dominated by the nonlocal contributions associated with the line-of-sight integrated electron overdensity, $\xi^{\rm lc\times lc}_{\rm XY}$ and display significant large-scale power. The relative amplitude of this contribution is consistent with the results of the angular power spectrum shown in Ref. [59]. The local density contribution ($\xi^{\rm l\times l}_{\rm XY}$) is a subdominant but non-negligible contribution to the monopole, depending on scales and redshift. These results on the even multipoles imply that the information of intrinsic three-dimensional distribution would become more subtle due to the light cone integral contributions, particularly at large scales. This fact differs from the case of RSDs, in which the even multipoles are primarily dominated by the local

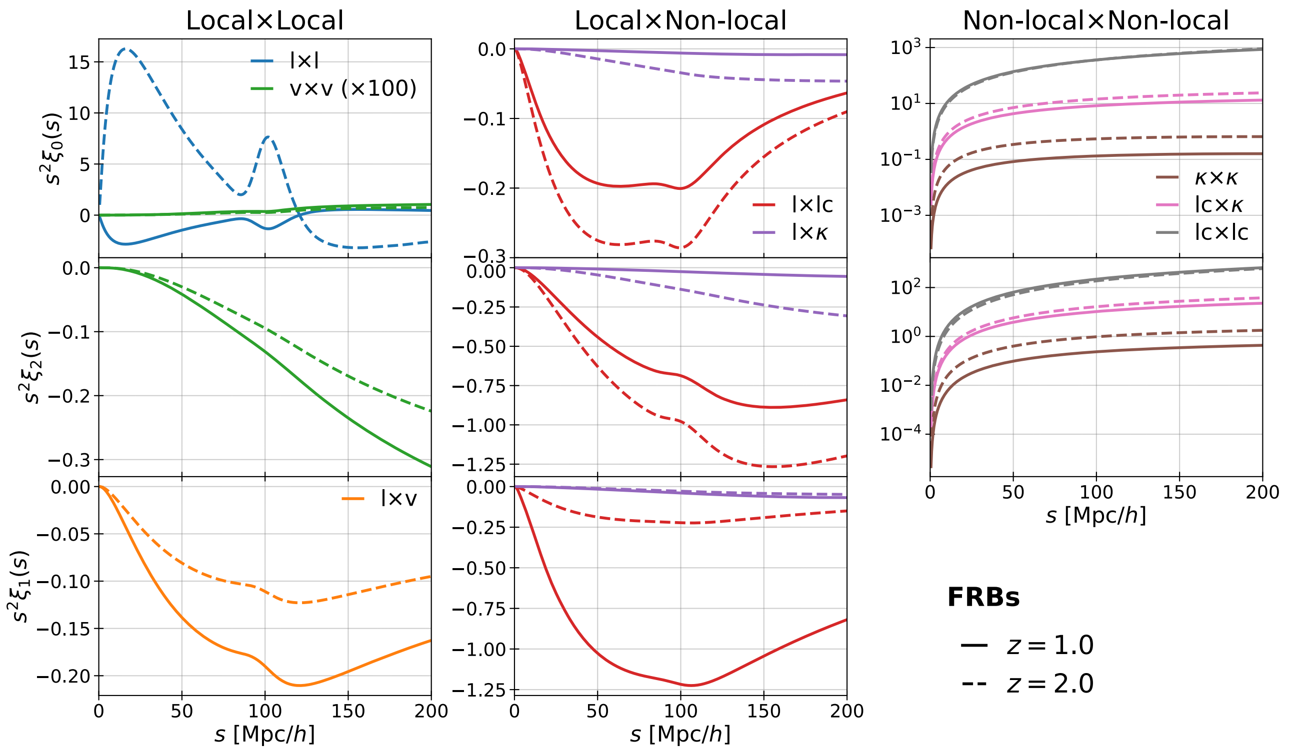

FIG. 1. Contributions to the multipoles at $z = 1.0$ (solid lines) and $z = 2.0$ (dashed lines). From left to right, we show the pure local, pure nonlocal, and crosstalk between the local and nonlocal contributions, respectively. From top to bottom, we present the monopole ($\ell = 0$), quadrupole ($\ell = 2$), and dipole ($\ell = 1$), respectively. For the bias parameter, we use Eqs. (33)–(35), and have $(b_{\rm X}, b_{\rm Y}) = (1.71, 0.71)$ for $z = 1.0$ and $(b_{\rm X}, b_{\rm Y}) = (3.15, 2.15)$ for $z = 2.0$. We set $f_{\rm s} = f_{\rm e} = 0$ and $b_e = 1$. For presentation purposes, we multiply the results for $\xi^{\rm v\times v}_{\rm XY}$ by 100 and plot the pure nonlocal contributions in log scale.

contributions. This systematic impact would be mitigated by looking at the small-scale behavior of the even multipoles. We note that the local density contribution becomes negative for $z = 1$ because it is proportional to $(b_{\rm X} - b_{\rm e})(b_{\rm Y} - b_{\rm e})$, and $b_{\rm Y} < b_{\rm e} = 1$ at $z = 1$. Turning to the dipole, all three contributions to the dipole have similar amplitudes. Among them, the cross-correlation between the local and nonlocal density terms ($\xi^{\rm l\times lc}_{\rm XY}$) is a major contributor at $z = 1$ but is suppressed at $z = 2$. Accordingly, the local velocity contribution, $\xi^{\rm l\times v}_{\rm XY}$, may dominate the dipole at high redshifts.

Figure 2 shows the redshift dependence of the multipoles at $s = 100$ Mpc$/h$. As we have already seen in Fig. 1, the even multipoles at low redshift $z \lesssim 3$ are dominated by the nonlocal density term ($\xi^{\rm lc\times lc}_{\rm XY}$). This makes it impossible to detect the baryon acoustic oscillations (BAO) feature in the FRB correlation function, for example, which is only present in correlations involving local contributions. Around $z \approx 3.8$, the contributions including the nonlocal density term become zero because of the vanishing factor $\mathcal{A}_{\rm X/Y} = 0$ [see Eq. (6)]. Around this specific redshift, since the nonlocal density contribution vanishes at all scales, the local contributions start to dominate the multipoles. We also find the other zero crossings at $z \approx 1.25$ in the monopole of $\xi^{\rm l\times l}_{\rm XY}$ and $z \approx 0.75$ in the quadrupole of $\xi^{\rm l\times lc}_{\rm XY}$,

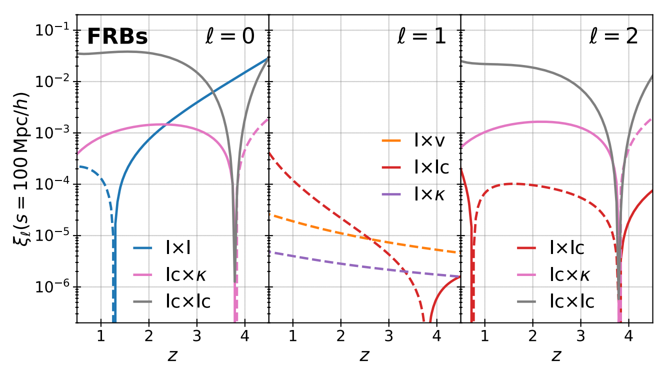

FIG. 2. First three dominant contributions to each multipole at $s = 100$ Mpc$/h$ as a function of redshift. From left to right, we show the monopole, dipole, and quadrupole, respectively. The dashed lines indicate the negative amplitude.

respectively. These zero-crossings correspond to the redshift satisfying $b_{\rm Y} - b_{\rm e} = 0$ in Eq. (21) and $(b_{\rm X} - b_{\rm e}) + (b_{\rm Y} - b_{\rm e}) = 0$ in Eq. (27) for the monopole and quadrupole, respectively. The local velocity contribution, which is always subdominant in the angular power spectrum [59], dominates the dipole at $z \gtrsim 3$. This would, in principle, allow us to isolate the local velocity term by studying three-dimensional clustering in DM space. It is important to

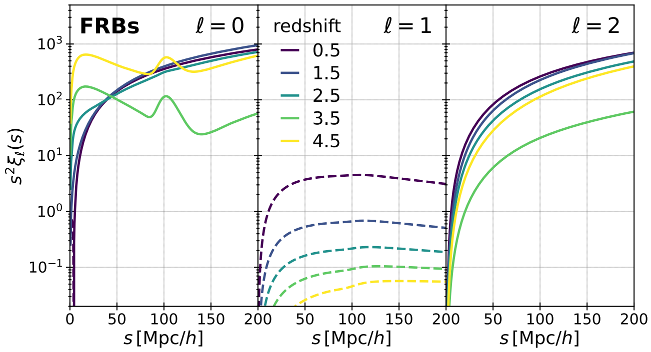

FIG. 3. Redshift evolution of the total signal of the multipoles. From left to right, we present the monopole, dipole, and quadrupole, respectively. For the bias parameters, we use the same setup in Figs. 1 and 2. The dashed lines indicate the negative amplitude.

emphasize that the occurrence of these zero crossings, our ability to isolate the velocity dipole, and to detect the BAO at high redshifts, are entirely dependent on the parametrizations assumed for all the astrophysical quantities entering our prediction (b_{X}, b_{e}, $\bar{n}_{\mathrm{e}}$, f_{e}, f_{X}) and are therefore subject to the current large uncertainties in the properties of FRB hosts.

Finally, we show the redshift dependence of the total signal for all multipoles in Fig. 3. The monopole shows a qualitatively different behavior at $z \lesssim 3.5$ and $z \gtrsim 3.5$, because the former is dominated by the nonlocal density contribution while the latter is dominated by the local density contribution, as seen in Fig. 2. Turning to the dipole, it monotonically decreases with increasing redshifts, as again expected from Fig. 2. The overall shape of the dipole does not drastically change because the two dominant contributions, $\xi^{\mathrm{l}\times\mathrm{v}}_{\mathrm{XY}}$ and $\xi^{\mathrm{l}\times\mathrm{lc}}_{\mathrm{XY}}$, display a similar behavior. As the quadrupole is mainly controlled by $\xi^{\mathrm{lc}\times\mathrm{lc}}_{\mathrm{XY}}$, it is suppressed around $z \approx 3.5$.

IV. GALAXY-FRB CROSS-CORRELATION FUNCTION

So far, we have investigated the anisotropy in the three-dimensional correlation function of FRBs measured in DM space, assuming that we obtain two different subsamples of FRBs, even though there is an inherent uncertainty in the splitting procedure. Moreover, the observed number of FRBs is expected to be smaller than that of galaxies. It is therefore interesting to consider the cross-correlation between FRBs and galaxies, which should be less sensitive to FRB shot noise and to our ability to subsample the FRB population in a meaningful way.

In the case of galaxies, the source's redshift is used as a distance proxy. The observed redshift is affected by various relativistic effects due to light propagation effects in an inhomogeneous universe, and these have been described and quantified in the literature (see, e.g., Refs. [61–64,77,80,85–88]). Considering the dominant contributions at linear order, the observed galaxy overdensity field in redshift space is given by [63,64,86]

$$\delta^{(\mathrm{S})}(\eta,\hat{\boldsymbol{n}}) = \delta^{\mathrm{l}}_{\mathrm{g}}(\eta,\hat{\boldsymbol{n}}) + \delta^{\mathrm{K}}_{\mathrm{g}}(\eta,\hat{\boldsymbol{n}}) + \delta^{\mathrm{v}}_{\mathrm{g}}(\eta,\hat{\boldsymbol{n}}) + \delta^{\kappa}_{\mathrm{g}}(\eta,\hat{\boldsymbol{n}}), \quad (36)$$

where we define

$$\delta^{\mathrm{l}}_{\mathrm{g}}(\eta,\hat{\boldsymbol{n}}) = b_{\mathrm{g}}\delta_{\mathrm{L}}(\boldsymbol{x}) \quad (37)$$

$$\delta^{\mathrm{v}}_{\mathrm{g}}(\eta,\hat{\boldsymbol{n}}) = \mathcal{B}(\chi)\delta^{\mathrm{v}}(\eta,\hat{\boldsymbol{n}}), \quad (38)$$

$$\delta^{\mathrm{K}}_{\mathrm{g}}(\eta,\hat{\boldsymbol{n}}) = -\frac{1}{\mathcal{H}}(\hat{\boldsymbol{n}}\cdot\boldsymbol{\nabla})(\boldsymbol{v}\cdot\hat{\boldsymbol{n}}), \quad (39)$$

$$\delta^{\kappa}_{\mathrm{g}}(\eta,\hat{\boldsymbol{n}}) = \delta^{\kappa}(\eta,\hat{\boldsymbol{n}}). \quad (40)$$

The quantities, δ^{v} and δ^{κ}, are defined in Eqs. (9) and (11), respectively. We introduced the linear galaxy bias parameter b_{g} and the time-dependent function $\mathcal{B}(\chi)$ given by

$$\mathcal{B}(\chi) = \left(-5s + \frac{5s-2}{\chi\mathcal{H}} - \frac{\dot{\mathcal{H}}}{\mathcal{H}^2} + f^{\mathrm{ev}}\right), \quad (41)$$

where the quantities s and f^{ev} are the magnification bias and evolution bias of galaxies, respectively. The terms on the right-hand side of Eq. (36) stand for the local density contribution, Kaiser effect [89,90], and Doppler contributions, and the lensing magnification contribution, respectively. Moving into Fourier space, the Kaiser term (39) becomes

$$\delta^{\mathrm{K}}(\eta,\hat{\boldsymbol{n}}) = f\int\frac{\mathrm{d}^3k}{(2\pi)^3}e^{i\boldsymbol{k}\cdot\boldsymbol{x}}(\hat{\boldsymbol{k}}\cdot\hat{\boldsymbol{n}})^2\delta_{\mathrm{L}}(\boldsymbol{k},\eta). \quad (42)$$

The expressions for $\delta^{\mathrm{l}}_{\mathrm{g}}$, $\delta^{\mathrm{v}}_{\mathrm{g}}$, and $\delta^{\kappa}_{\mathrm{g}}$ in Fourier space are given in Eqs. (12), (13), and (15), respectively.

Using this notation, we calculate the cross-correlation between galaxies and FRBs,

$$\xi_{\mathrm{gX}}(\boldsymbol{x}_1,\boldsymbol{x}_2) = \left\langle\delta^{(\mathrm{S})}_{\mathrm{g}}(\boldsymbol{x}_1)\delta^{(\mathcal{D})}_{\mathrm{X}}(\boldsymbol{x}_2)\right\rangle. \quad (43)$$

Here, in order to distinguish from the notation of the FRB cross-correlation function ξ_{XY}, we denote the FRB-galaxy cross-correlation function ξ_{gX} where X represents FRBs having the bias parameter b_{X}. We omit the time dependence in the notations for simplicity.

Substituting Eqs. (37)–(40) into Eq. (43), we derive the analytical expression for the galaxy-FRB cross-correlation function. Similar to the FRB correlation function, we split the galaxy-FRB correlation function into nine pieces,

$$\xi_{\mathrm{gX}} = \left(\xi^{\mathrm{l}\times\mathrm{l}}_{\mathrm{gX}} + \xi^{\mathrm{l}\times\mathrm{v}}_{\mathrm{gX}} + \xi^{\mathrm{v}\times\mathrm{v}}_{\mathrm{gX}} + \xi^{\mathrm{K}\times\mathrm{l}}_{\mathrm{gX}} + \xi^{\mathrm{K}\times\mathrm{v}}_{\mathrm{gX}}\right) + \left(\xi^{\mathrm{lc}\times\kappa}_{\mathrm{gX}} + \xi^{\kappa\times\kappa}_{\mathrm{gX}}\right) + \left(\xi^{\mathrm{l}\times\mathrm{lc}}_{\mathrm{gX}} + \xi^{\mathrm{l}\times\kappa}_{\mathrm{gX}}\right), \quad (44)$$

where we define

$$\xi_{\rm gX}^{\rm a\times b} = \langle \delta_{\rm g}^{\rm a}(\boldsymbol{x}_1)\delta_{\rm X}^{\rm b}(\boldsymbol{x}_2)\rangle + ({\rm a}\leftrightarrow{\rm b}), \tag{45}$$

for $({\rm a},{\rm b}) = ({\rm l},{\rm v}),({\rm l},\kappa),({\rm v},\kappa)$, and otherwise,

$$\xi_{\rm gX}^{\rm a\times b} = \langle \delta_{\rm g}^{\rm a}(\boldsymbol{x}_1))\delta_{\rm X}^{\rm b}((\boldsymbol{x}_2))\rangle. \tag{46}$$

In Eq. (44), the first, second, and third parentheses on the right-hand side, respectively, correspond to the pure local contributions, the pure nonlocal contributions, and the cross-correlation between local and nonlocal terms. Similar to the FRB cross-correlation function, the cross-contributions between the local velocity or Kaiser terms and nonlocal terms vanish in the Limber approximation, i.e., $\langle\delta_{\rm g}^{\rm v}\delta_{\rm X}^{\rm lc}\rangle = \langle\delta_{\rm g}^{\rm K}\delta_{\rm X}^{\rm lc}\rangle = \langle\delta_{\rm g}^{\rm v}\delta_{\rm X}^{\kappa}\rangle = \langle\delta_{\rm g}^{\rm K}\delta_{\rm X}^{\kappa}\rangle = 0$. The explicit forms of each contribution are given by

$$\xi_{\rm gX}^{\rm l\times l} = b_{\rm g}(b_{\rm X}-b_{\rm e})\Xi_0^{(0)}(\eta,s), \tag{47}$$

$$\xi_{\rm gX}^{\rm l\times v} = -[b_{\rm g}-\mathcal{B}(\chi)(b_{\rm X}-b_{\rm e})]\mu(s\mathcal{H}f)\Xi_1^{(1)}(\eta,s), \tag{48}$$

$$\xi_{\rm gX}^{v\times v} = \mathcal{B}(\chi)(s\mathcal{H}f)^2\left[\left(\frac{1}{3}-\mu^2\right)\Xi_2^{(2)}(\eta,s)+\frac{1}{3}\Xi_0^{(2)}(\eta,s)\right], \tag{49}$$

$$\xi_{\rm gX}^{\rm K\times l} = f(b_{\rm X}-b_{\rm e})\left[\left(\frac{1}{3}-\mu^2\right)\Xi_2^{(0)}(\eta,s)+\frac{1}{3}\Xi_0^{(0)}(\eta,s)\right], \tag{50}$$

$$\xi_{\rm gX}^{{\rm K}\times v} = \mathcal{H}sf^2\left[\left(\mu^3-\frac{3}{5}\mu\right)\Xi_3^{(1)}(\eta,s)-\frac{3}{5}\mu\Xi_1^{(1)}(\eta,s)\right], \tag{51}$$

for the purely local contributions,

$$\begin{aligned}\xi_{\rm gX}^{{\rm lc}\times\kappa} &= -\mathcal{A}_{\rm X}(\chi)b_{\rm e}\frac{\mathcal{H}}{a^2\bar{n}_{\rm e}}\frac{3\Omega_{\rm m0}\mathcal{H}_0^2}{\chi}\int_0^\chi {\rm d}\chi' a(\chi')\bar{n}_{\rm e}(\chi')\\ &\quad\times(\chi-\chi')\chi'\mathcal{J}\left(\eta',\frac{\chi'}{\chi}s\sqrt{1-\mu^2}\right),\end{aligned} \tag{52}$$

$$\begin{aligned}\xi_{\rm gX}^{\kappa\times\kappa} &= \left(\frac{3\Omega_{\rm m0}\mathcal{H}_0^2}{\chi}\right)^2\int_0^\chi {\rm d}\chi'\left(\frac{(\chi-\chi')\chi'}{a(\chi')}\right)^2\\ &\quad\times\mathcal{J}\left(\eta',\frac{\chi'}{\chi}s\sqrt{1-\mu^2}\right),\end{aligned} \tag{53}$$

for the purely nonlocal contributions, and

$$\xi_{\rm gX}^{\rm l\times lc} = \Theta(\chi_2-\chi_1)b_{\rm g}b_{\rm e}\mathcal{A}_{\rm X}(\chi)\mathcal{H}\mathcal{J}\left(\eta,s\sqrt{1-\mu^2}\right), \tag{54}$$

$$\begin{aligned}\xi_{\rm gX}^{{\rm l}\times\kappa} &= (-\Theta(\chi_2-\chi_1)b_{\rm g}+\Theta(\chi_1-\chi_2)(b_{\rm X}-b_{\rm e}))\\ &\quad\times\frac{3\Omega_{\rm m0}\mathcal{H}_0^2}{a}s\mu\mathcal{J}\left(\eta,s\sqrt{1-\mu^2}\right),\end{aligned} \tag{55}$$

for the cross-correlation between them.

We quantify the anisotropy in the galaxy-FRB cross-correlation function by performing the multipole expansion (31) and present the first three multipoles in Fig. 4. We first focus on the even multipoles. There are two dominant contributions: the purely local $\xi_{\rm gX}^{\rm l\times l}$, and the purely nonlocal $\xi_{\rm gX}^{{\rm lc}\times\kappa}$, which captures the correlation between magnification bias and the integrated electron density. The absence of the dominant $\xi_{\rm XY}^{\rm lc\times lc}$ in the FRB-only (see Fig. 1) makes it now possible to observe features like the BAO peak in the cross-correlation with galaxies (albeit with a significant nonlocal contribution). We further find that the contribution from the Kaiser term, which is a unique effect in the galaxy-FRB cross-correlation, is subdominant in the monopole but plays an important role in the quadrupole, especially, at higher redshifts. Turning to the dipole, the primary contributor is $\xi_{\rm gX}^{\rm l\times lc}$ at $z=1$ and $\xi_{\rm gX}^{\rm l\times v}$ at $z=2$. The Kaiser term is a minor contribution to the dipole.

Figure 5 shows the redshift-dependence of the first three dominant contributions to the multipoles. Similar to the FRB-only case, shown in Fig. 2, the contributions including the nonlocal density term vanish around $z\approx 3.8$, where $\mathcal{A}_{\rm X}\approx 0$. Since the contributions $(\xi_{\rm gX}^{\rm l\times l},\xi_{\rm gX}^{\rm K\times l})$ and $(\xi_{\rm gX}^{\rm l\times v},\xi_{\rm gX}^{{\rm l}\times\kappa})$ are, respectively, proportional to the factor $b_{\rm X}-b_{\rm e}$ and $b_{\rm g}-(b_{\rm X}-b_{\rm e})$, they vanish around $z\approx 0.75$ and $z\approx 0.5$, respectively, in the present setup of the bias parameter (33). The even multipoles are dominated by the local density and Kaiser terms at all redshifts, while the dipole is dominated by the local velocity term at higher redshift and the nonlocal density term at lower redshift (similar to the FRB-only case). This suggests that it may be possible to isolate and detect the relativistic Doppler contribution from the dipole, assuming that the various astrophysical quantities entering $\mathcal{A}_{\rm X}$ and $\mathcal{B}$ can be determined with sufficient precision.

Finally, we present the behavior of the total signal in Fig. 6, which is directly related to the behavior seen in Fig. 5. At the lowest redshift, the even multipoles show a complex scale dependence due to the coexistence of contributions of different signs, whereas at high redshift, the correlation function multipoles can be explained solely in terms of the $\xi_{\rm gX}^{\rm l\times l}$ and $\xi_{\rm gX}^{\rm K\times l}$ terms. The redshift dependence of the dipole does not drastically change compared to the even multipoles due to the two similar contributions, $\xi_{\rm gX}^{\rm l\times v}$ and $\xi_{\rm gX}^{\rm l\times lc}$. High redshift observations of the monopole, dipole, and quadrupole provide us with information about the local density, Doppler effect, and Kaiser effect contributions, suggesting that the three-dimensional clustering in DM space may be a useful cosmological probe, complementary to galaxy redshift surveys.

V. FUTURE DETECTABILITY

As demonstrated above, the anisotropic signal in the FRB correlation function in DM space may provide a complementary method to test our cosmological model and

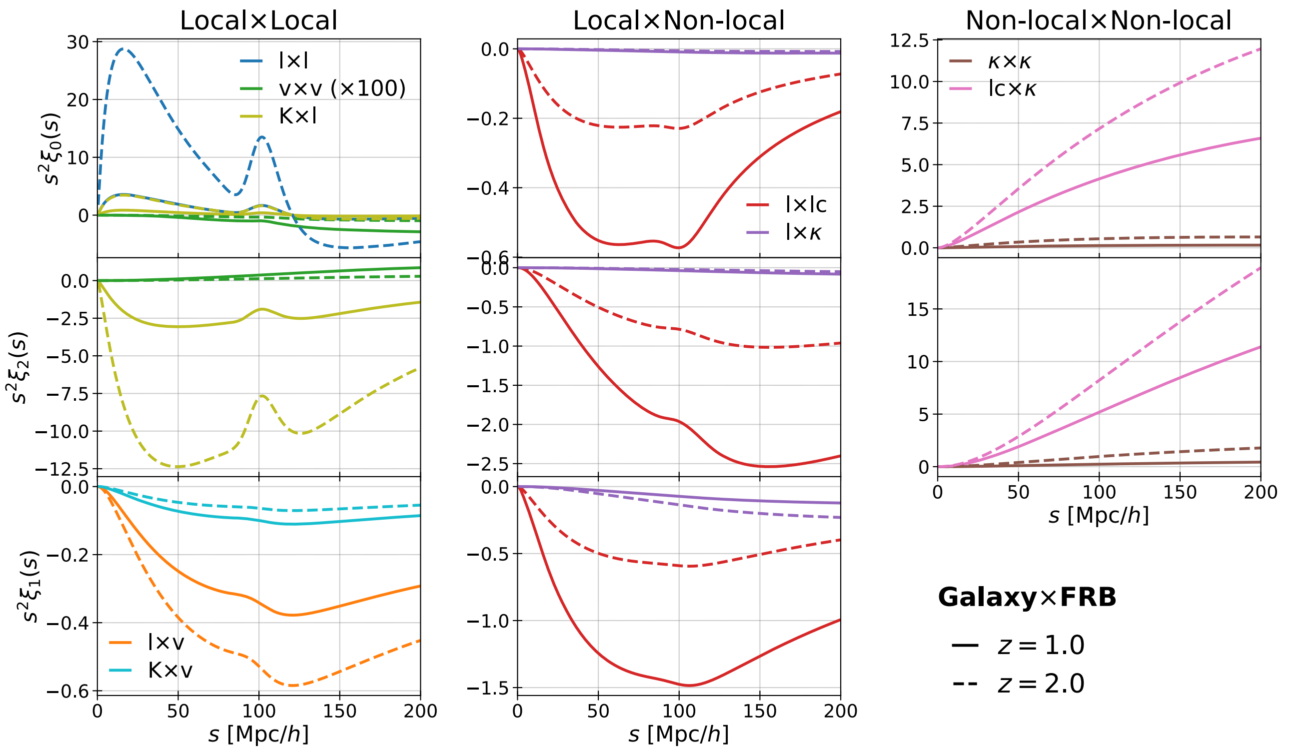

FIG. 4. Same as Fig. 1 but for the galaxy-FRB cross-correlations. The result of $\xi_{\rm gX}^{\rm v\times v}$ is multiplied by a factor of 100 for presentation purposes. The bias parameters follow the HI galaxies observed by SKA2, i.e., $b_{\rm SKA}(z) = b_{\rm g} = b_{\rm FRB}$, defined in Eq. (33).

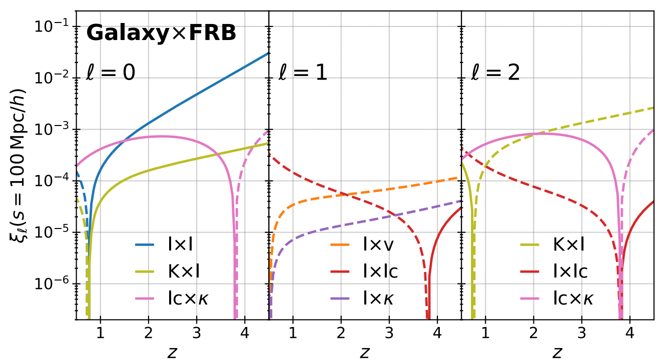

FIG. 5. Same as Fig. 2 but for the galaxy-FRB cross-correlations.

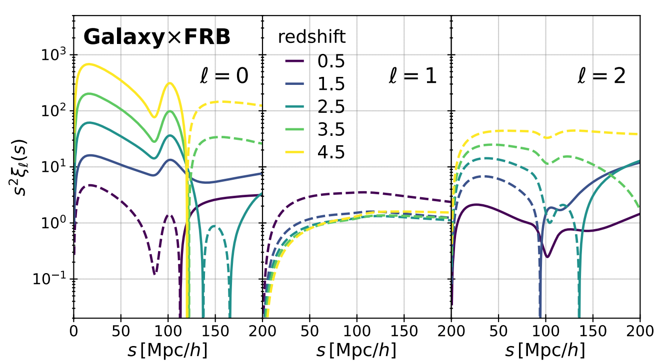

FIG. 6. Same as Fig. 3 but for the galaxy-FRBs cross-correlations.

theory of gravity. In this section, we perform a Fisher matrix analysis to investigate the future detectability of this signal, assuming an SKA-like survey specification, assuming the detection of a large number of FRBs. To this end, it is more convenient to work with two-point statistics in Fourier space than in real space. Thus, we first define the multipole power spectrum in Sec. V A, and investigate their detectability in Sec. V B.

A. Power spectrum multipoles

The power spectrum multipoles are related to the multipoles of the correlation function via

$$P_\ell(k) = 4\pi(-i)^\ell \int {\rm d}s\, s^2 j_\ell(ks)\xi_\ell(s), \tag{56}$$

where we still take the distant-observer limit. To compute the multipole power spectrum, we perform this integral numerically.

In Fig. 7, we present the multipole power spectra at $z = 1$ and 2. These results are simply the Fourier counterpart of the correlation function results shown in Figs. 1 and 4. We see again that the even multipoles of the FRB power spectra (top panels) are dominated by the pure nonlocal contribution whereas the dipole is not because of the absence of the nonlocal density contribution. Likewise, the purely nonlocal contribution to the galaxy-FRB

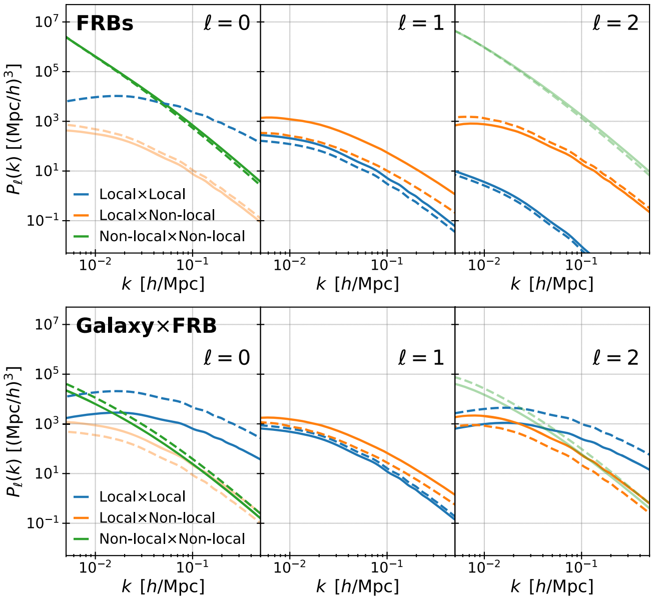

FIG. 7. Power spectrum multipoles for the FRB power spectra (top panels) and galaxy-FRB cross-power spectra (bottom panels) at $z = 1$ (solid lines) and at $z = 2$ (dashed lines). The thin lines indicate a negative amplitude. Blue, orange, and green lines, respectively, show the sum of the pure local contributions, crosstalk between the local and nonlocal contributions, and pure nonlocal contributions.

cross-power spectra (bottom panels) is suppressed compared to the FRB-only case. The behavior of the monopole in the FRB power spectra is consistent with the angular power spectrum predictions found in Ref. [59].

B. Signal-to-noise ratio

In this subsection, we discuss the future detectability of DM-space anisotropies. To estimate the signal-to-noise ratio, we compute the covariance matrix of the power spectrum multipoles between the objects X and Y by neglecting the non-Gaussian contribution (e.g., Refs. [70,91–93]),

$$\mathrm{COV}_\ell(k, k') \equiv \left\langle \Delta P_\ell^{\mathrm{XY}}(k)(\Delta P_\ell^{\mathrm{XY}}(k'))^* \right\rangle \tag{57}$$

$$\equiv \frac{\delta_{\mathrm{D}}(k - k')}{k^2} \frac{2\pi^2}{V} \sigma_\ell^2(k), \tag{58}$$

where, we have defined the variance $\sigma_\ell^2(k)$ as

$$\sigma_\ell^2(k) = \frac{1}{2} \sum_{\ell_1, \ell_2} \left[\left(P_{\ell_1}^{\mathrm{XX}}(k) + \frac{\delta_{\ell_1,0}}{n_{\mathrm{X}}} \right) \left(P_{\ell_2}^{\mathrm{YY}}(k) + \frac{\delta_{\ell_2,0}}{n_{\mathrm{Y}}} \right) + (-1)^\ell P_{\ell_1}^{\mathrm{XY}}(k) P_{\ell_2}^{\mathrm{YX}}(k) \right] \left(\frac{2\ell + 1}{2} \right)^2 \times \int \mathrm{d}\mu \mathcal{L}_\ell(\mu) \mathcal{L}_\ell(\mu) \mathcal{L}_{\ell_1}(\mu) \mathcal{L}_{\ell_2}(-\mu). \tag{59}$$

Here, the quantities $n_{\mathrm{X/Y}}$ and V stand for the number density of the X/Y samples, and the observed volume, respectively. We numerically compute the multipole power spectrum by Eq. (56).

In the signal-to-noise ratio analysis, we consider two cases: FRB cross-power spectrum and galaxy-FRB cross-power spectrum. As we expect to detect roughly 10^5–10^6 FRBs in the SKA era [15], we set the number of FRBs of each species to 10^4–10^6. We use the galaxy number density given by the specifications of SKA2 HI galaxies in Eq. (B1) in Ref. [84],

$$\frac{\mathrm{d}N}{\mathrm{d}z} = 10^{c_1} z^{c_2} \exp(-c_3 z) \quad [\mathrm{deg}^{-2}], \tag{60}$$

with $c_1 = 6.319$, $c_2 = 1.736$, and $c_3 = 5.424$. The average number of galaxies per redshift interval can be related to the number density per volume by $n = \mathrm{d}N/\mathrm{d}z(\Delta z f_{\mathrm{sky}}/V)$ with $\Delta z = 0.1$ and $f_{\mathrm{sky}} = 30000\ \mathrm{deg}^2$ being the width of redshift bins and the fractional sky coverage, respectively. We compute the survey volume as $V = 4\pi/3(\chi(z + \Delta z/2)^3 - \chi(z - \Delta z/2)^3)$. Note that, optimistically, we assume that all the detected FRBs are located within the same $\Delta z = 0.1$ interval. In computing the galaxy auto-power spectrum entering the covariance, we ignore the negligible small contribution from relativistic effects [82,88,94] and simply consider the standard Kaiser effect. We then estimate the signal-to-noise ratio by

$$\left(\frac{\mathrm{S}}{\mathrm{N}}\right)^2 = \int_{k_{\min}}^{k_{\max}} \mathrm{d}k\, P_\ell^{\mathrm{XY}}(k) [\mathrm{COV}_\ell(k, k')]^{-1} (P_\ell^{\mathrm{XY}}(k'))^* = V \int_{k_{\min}}^{k_{\max}} \frac{\mathrm{d}k}{2\pi^2} k^2 \frac{|P_\ell^{\mathrm{XY}}(k)|^2}{\sigma_\ell^2(k)}, \tag{61}$$

where we set $k_{\min} = 2\pi V^{-1/3}$ and $k_{\max} = 0.1\ h/\mathrm{Mpc}$ to avoid the nonlinear contribution to the density perturbations (see Appendix B for the nonlinear contributions to the dipole).

Using Eq. (61), we compute the redshift dependence of the signal-to-noise ratio of the multipole power spectra assuming the SKA-like survey, shown in Fig. 8. We found that the even multipole power spectra could be detected with the high statistical significance, $\mathrm{S/N} \approx 10^1$–$10^2$. Interestingly, we observe a suppression of the signal-to-noise ratio at $z \approx 3.8$ in the quadrupole of the FRB alone result. This is because the quadrupole is dominated by the nonlocal density term, which becomes zero around $z \approx 3.8$ (see Fig. 3). Overall, the signal-to-noise ratio for the even multipoles in the FRB-only case is larger than that of the cross-power spectra case, mostly due to the purely nonlocal density term $\xi_{\mathrm{XY}}^{\mathrm{lc \times lc}}$, which significantly amplifies the even multipole signal.

Turning to the signal-to-noise ratio for the dipole, observations at low redshift have the best chances of

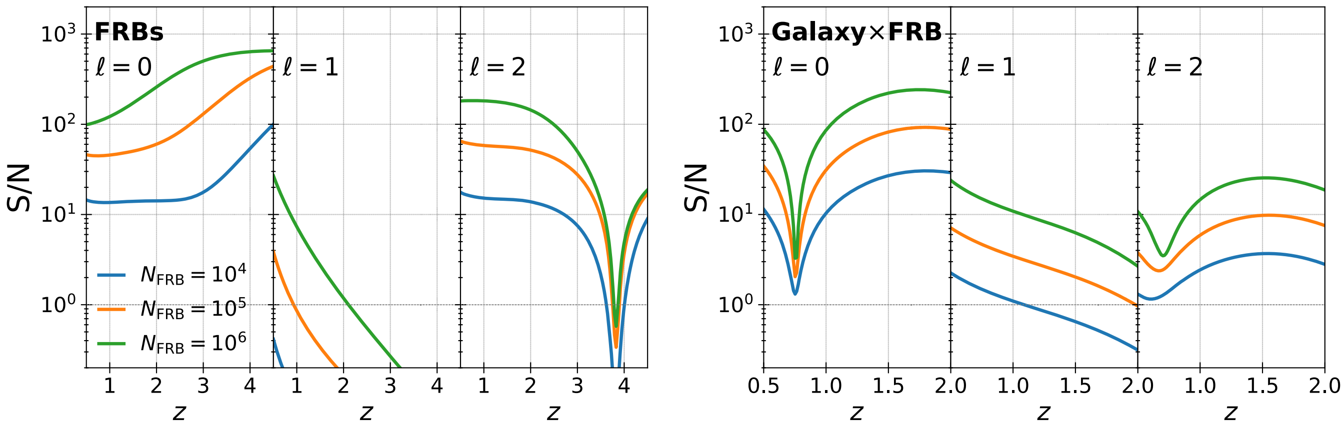

FIG. 8. Signal-to-noise ratio of the multipole power spectra in the SKA-like survey specifications for FRBs power spectra (left panels) and for galaxy-FRB cross-power spectra (right panels), respectively. The blue, orange, and green lines represent, respectively, the results with the number of FRBs, $N_{\mathrm{FRB}} = 10^4$, 10^5, and 10^6.

detecting the dipole, although in this case the dipole is dominated by not the relativistic effect but the nonlocal density contribution. However, assuming a more optimistic number of FRBs $\sim 10^6$, the chance for detecting the relativistic effect through the dipole improves more, with $\mathrm{S/N} \gtrsim 1$ at $z \approx 2$. Moreover, cross-correlations between FRBs and galaxies, the signal-to-noise ratio of the dipole improves, particularly $\mathrm{S/N} \approx 10$ for the most optimistic case with $N_{\mathrm{FRB}} = 10^6$. Hence, observing a large number of FRBs and making a three-dimensional map of FRBs may be an interesting new approach to the detection of relativistic effects. In addition, the even multipole anisotropy in DM space contains a wealth of cosmological information, which would also provide complementary information to galaxy redshift surveys.

VI. SUMMARY

We have investigated the three-dimensional clustering of the sources emitting electromagnetic pulses such as fast radio bursts (FRBs) in dispersion measure (DM) space. The DM of pulses can be exploited as a cosmological distance measure, although it is systematically affected by inhomogeneities in the electron density and special and general relativistic effects, as is the redshift measured in galaxy redshift surveys. Accordingly, the observed DM-based clustering is affected by DM space distortions. Following the footsteps of Refs. [32,36,57,58], we formulate the two-point statistics in DM space including all the possible dominant contributions to the DM.

The observed anisotropy in the correlation function or power spectrum is induced by the contributions from the nonlocal integral term along the line of sight and from the Doppler term, which is a major relativistic contribution to the DM. Performing a multipole expansion, we found that the even multipoles are primarily dominated by both the nonlocal density and local density contributions, whereas the dipole moment receives a contribution from the Doppler term, suggesting that observing three-dimensional clustering may isolate this relativistic effect. We note that, as in the case of redshift space distortions, the nonvanishing dipole appears only when we correlate two different biased objects, i.e., cross correlation between two subsamples of FRBs with different biases or galaxy-FRB cross correlation.

Based on the derived analytical model for the correlation function or power spectrum in DM space, we further investigate the future detectability by performing the Fisher matrix analysis. Assuming an SKA-like survey, the signal-to-noise ratio for the even multipoles reaches $\mathrm{S/N} \approx 100$ and that the dipole may be detectable if a sufficiently large number of FRBs are measured. In the optimistic case where the observed number of FRBs is 10^5–10^6, the signal-to-noise ratio exceeds unity even at high redshift, where the Doppler term dominates the dipole, and hence, the high-redshift measurement would be an interesting probe to test gravity, complementary to galaxy redshift surveys.

In the Fisher matrix analysis, we have made several simplifications to make the problem more tractable. Importantly, we have ignored the local contribution to the DM from the electron density of host galaxies. With the simplified demonstration in Appendix C, this contribution leads to the suppression of the correlation signal at small scales if its contribution is a random quantity uncorrelated to the large-scale structure [70], effectively increasing the uncertainty in the measurement. This assumption could be refined, for example, through the use of hydrodynamic simulations (e.g., Refs. [44,95,96]), providing a more realistic forecast. We have also assumed a relatively high number density of FRBs, and thus, the results presented depend on the ability of future experiments, such as the SKA, to achieve this detection rate. Finally, we have set the bias parameter of FRBs to be similar to that of the HI galaxies observed by SKA2.

Furthermore, we have ignored the gravitational potential contribution to the DM as it is expected to be negligible at large scales. However, if FRBs reside in the deep potential well of dark matter haloes, the gravitational potential contribution would play a certain role at small scales (see redshift-space examples [79,81–83]). Properly taking into account these contributions, the anisotropy of the three-dimensional clustering in DM space could become a more promising and robust probe for testing gravity on cosmological scales in the next decades.

ACKNOWLEDGMENTS

We would like to thank Francesca Lepori and Ruth Durrer for interesting discussions. This work is supported by the Japan Society for the Promotion of Science (JSPS) Overseas Research Fellowships, the JSPS KAKENHI Grant No. 23K19050 and No. 24K17043 (S. S.). S. S. thanks Julien Devriendt for being a host during the Balzan program. This work was initiated during the visiting program supported by a Centre for Cosmological Studies Balzan Fellowship.

APPENDIX A: WIDE-ANGLE CORRECTION

Here, we derive the wide-angle correction to the local contributions. Since the wide-angle correction to the nonlocal contribution would be negligible for the multipole analysis [68,75], we focus only on the local contributions here.

In general, the correlation function is given as a function of two vectors $\boldsymbol{x}_1$ and $\boldsymbol{x}_2$, but the correlation function in the distant observer limit can be given as a function of the separation $s = |\boldsymbol{x}_2 - \boldsymbol{x}_1|$ and the directional cosine between the separation vector and the fixed line-of-sight vector: $\mu = \hat{\boldsymbol{n}} \cdot \hat{z}$. However, when we do not take the distant observer limit, the correlation function can be characterized by three variables: the separation s, line-of-sight distance specifically pointing to a midpoint $\chi = |\boldsymbol{d}| = |\boldsymbol{x}_1 + \boldsymbol{x}_2|/2$, and directional cosine between the separation vector and the line-of-sight vector $\mu = \hat{\boldsymbol{n}} \cdot \hat{\boldsymbol{d}}$, i.e., $\xi(\boldsymbol{x}_1, \boldsymbol{x}_2) = \xi(x, \chi, \mu)$.

We then expand the correlation function in powers of (s/χ) to split the χ dependence from the correlation function as follows:

$$\xi(s, \chi, \mu) = \xi^{(\mathrm{pp})}(s, \mu) + \xi^{(\mathrm{wa})}(s, \mu) + O\left(\left(\frac{s}{\chi}\right)^2\right), \tag{A1}$$

where the first and second terms on the right-hand side are, respectively, the expression in the distant observer limit ($s/\chi \to 0$), and the leading-order correction to the wide-angle effect $\propto (s/\chi)^1$.

First, we look at the wide-angle correction to the FRB cross-correlation. Among the local contributions, only the cross-correlation between δ^{l} and δ^{v} has a nonvanishing wide-angle correction $O(s/\chi)$, which is explicitly given by

$$\xi_{\mathrm{XY}}^{\mathrm{l}\times\mathrm{v},(\mathrm{wa})} = \left(\frac{s}{\chi}\right)(b_{\mathrm{X}} + b_{\mathrm{Y}} - 2b_{\mathrm{e}}) \times \left(\mu^2 - \frac{1}{2}\right)(s\mathcal{H}f)\Xi_1^{(1)}(\eta, s). \tag{A2}$$

Next, for the galaxy-FRBs cross-correlation case, the nonvanishing wide-angle corrections at the leading order are given by

$$\xi_{\mathrm{gX}}^{\mathrm{K}\times\mathrm{l},(\mathrm{wa})} = \left(\frac{s}{\chi}\right) f(b_{\mathrm{X}} - b_{\mathrm{e}})(1 - 2\mu^2)\mu\Xi_2^{(0)}(\eta, s), \tag{A3}$$

$$\xi_{\mathrm{gX}}^{\mathrm{K}\times\mathrm{v},(\mathrm{wa})} = \left(\frac{s}{\chi}\right) s\mathcal{H}f^2\left(\mu^2 - \frac{1}{2}\right) \times \left[\mu^2\Xi_3^{(1)}(\eta, s) - \Xi_2^{(2)}(\eta, s)\right]. \tag{A4}$$

Using the derived analytical expressions, we compare the wide-angle correction to the total local contributions in Fig. 9. Clearly, the wide-angle contribution to the galaxy-FRB cross-correlation is negligibly small compared

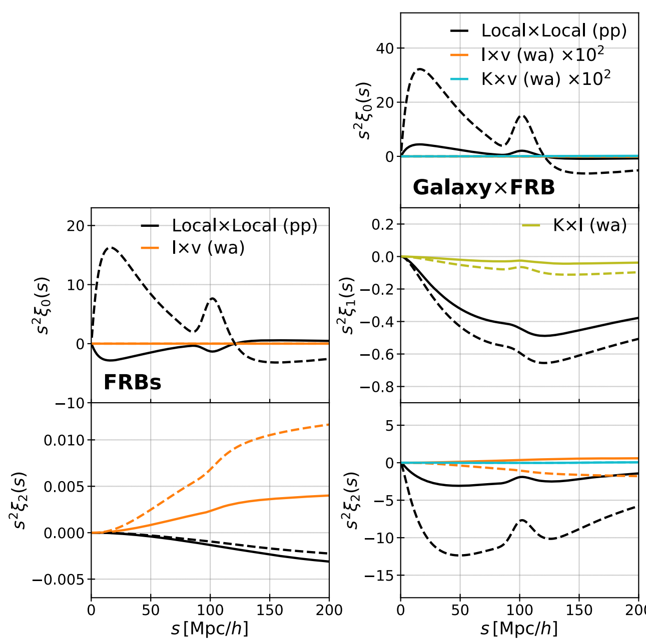

FIG. 9. Wide-angle corrections to the multipoles of the FRBs cross-correlation function at $z = 1.0$ (solid lines) and at $z = 2.0$ (dashed lines). The black lines present the total local contributions, i.e., the sum of Eqs. (21)–(23) for the FRB alone case and the sum of Eqs. (47)–(51) for the galaxy-FRB cross-correlation case. For presentation purposes, the results in the right panels for $\xi_{\mathrm{gX}}^{\mathrm{l}\times\mathrm{v},(\mathrm{wa})}$ and $\xi_{\mathrm{gX}}^{\mathrm{K}\times\mathrm{v},(\mathrm{wa})}$ are multiplied by 10^2.

to the result of the plane-parallel limit. On the other hand, the wide-angle correction to the quadrupole of the FRB cross-correlation exhibits a non-negligible impact. However, the total quadrupole signal is mostly dominated by the nonlocal contributions, as far as we are interested in the total signal, the wide-angle correction can be safely ignored.

APPENDIX B: NONLINEAR IMPACT ON THE DIPOLE SIGNAL

As we have shown in Figs. 1 and 4, the cross-correlation between the local and nonlocal terms is the dominant contributor to the dipole signal. In this appendix, we discuss the impact of the nonlinear density growth on the dipole signal, particularly focusing on the local and nonlocal crosstalk.

To include the nonlinear density growth into the prediction, we simply replace the linear matter power spectrum in $\Xi_\ell^{(n)}$ and $\mathcal{J}$, respectively given in Eqs. (29) and (30), by the nonlinear matter power spectrum computed by using `CLASS` with a nonlinear output option `HALOFIT` [97,98]. Figure 10 show the impact of the nonlinear matter power spectrum on the dipole signal. As we clearly see that, as long as we restrict our analysis to the large-scale signal, we safely ignore the nonlinear matter growth effect because it suppresses the dipole signal only a few percent level at $s \gtrsim 20\ \mathrm{Mpc}/h$.

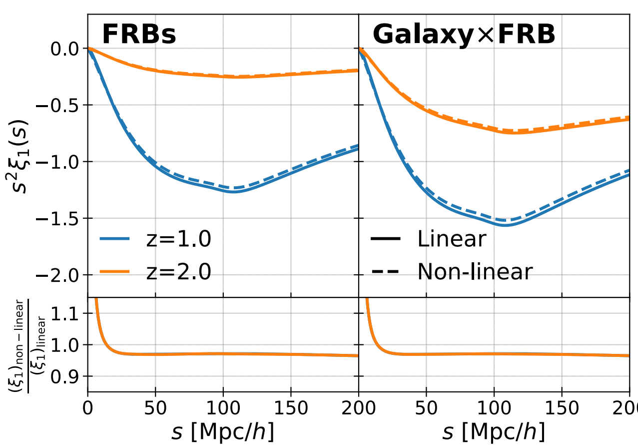

FIG. 10. Dipole from the cross correlation between the local and nonlocal terms at $z = 1.0$ (blue) and $z = 2.0$ (orange). The solid and dashed lines represent, respectively, the prediction with the linear matter power spectrum and with the nonlinear matter power spectrum. The bottom panels show the ratio between the predictions with the linear and nonlinear matter power spectrum. We note that the blue and orange lines in the bottom panels mostly overlap, and only the orange lines are visible.

APPENDIX C: CONTRIBUTION FROM HOST GALAXIES

In this appendix, we discuss the impact of free electrons in host galaxies on the correlation functions. As the FRBs generally resides in galaxies, where non-negligible amount of free electrons present, the observed DM would be given by

$$\mathcal{D}_{\rm obs} = \mathcal{D}_{\rm cos} + \mathcal{D}_{\rm host}, \tag{C1}$$

where the cosmological DM, $\mathcal{D}_{\rm cos}$, represents the DM from the propagation of the FRB pulse through the inhomogeneous universe, which we have investigated in the main text. On top of the cosmological DM, the host galaxy contribution, $\mathcal{D}_{\rm host}$, which is always positive, should be added. Realistically, the host galaxy contributions would be larger (smaller) for more (less) massive halos and would correlate to the cosmological components across large distances. However, in order to make the problem tractable, we simply assume that the host galaxy contribution does not correlate to the cosmological contribution and obeys a certain distribution function, $f(\mathcal{D}_{\rm host})$. This correlation would be interesting to investigate in the future with simulations. Using Eq. (4), the presence of the additive contribution to the DM leads to the following modification in the comoving distance:

$$\Delta\chi(z, D_{\rm host}) \simeq \frac{\mathcal{D}_{\rm host}}{a^2(z)\bar{n}_{\rm e}(z)}, \tag{C2}$$

where we used the definition of the comoving distance, $\chi(z) = \int_0^z \mathrm{d}z' H^{-1}(z')$. As $\mathcal{D}_{\rm host}$ is always positive, the induced shift is also positive. Due to the host galaxy contribution to the DM, the position of FRBs in the DM space is always shifted to a more distant location.

We now include this additive term arising from the host galaxy's DM into the analytical model of the correlation functions. First, we consider the pure local contribution, which is schematically given in the distant-observer limit by

$$\xi^{\rm Local\times Local} = \int \frac{\mathrm{d}^3\boldsymbol{k}}{(2\pi)^3} e^{i\boldsymbol{k}\cdot\boldsymbol{s}} P(k, \hat{\boldsymbol{k}}\cdot\hat{\boldsymbol{z}}). \tag{C3}$$

In the presence of $\mathcal{D}_{\rm host}$, the separation vector in the exponent is modified by $\boldsymbol{s} \to (s + \Delta\chi)\hat{\boldsymbol{s}}$ with $\Delta\chi > 0$. This results in the modification: $\Xi_\ell^{(n)}(s) \to \Xi_\ell^{(n)}(s + \Delta\chi)$ in the analytical expression of the correlation functions. Taking into account the distribution of $\mathcal{D}_{\rm host}$, we can replace $\Xi_\ell^{(n)}(s)$ in the pure local contributions by

$$\tilde{\Xi}_\ell^{(n)}(s) = \int_0^\infty \mathrm{d}\mathcal{D}_{\rm host} \Xi_\ell^{(n)}(s + \Delta\chi(z, D_{\rm host})) f(\mathcal{D}_{\rm host}). \tag{C4}$$

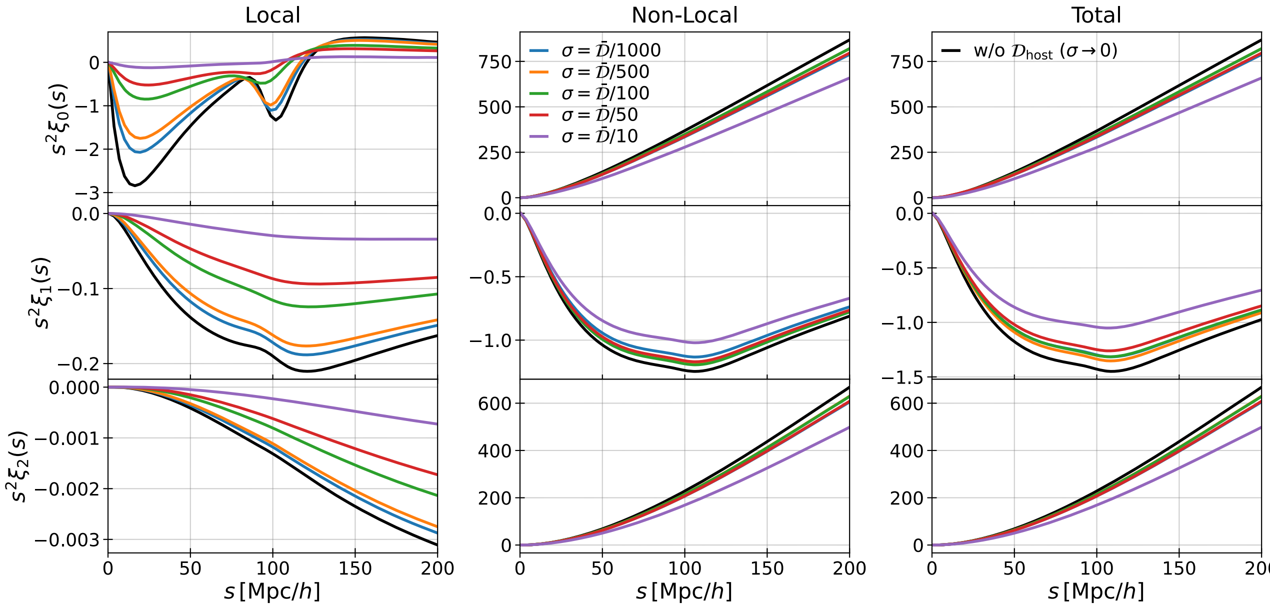

FIG. 11. Impact of the halo contribution to the multipoles of FRBs cross-correlation function at $z = 1.0$ assuming the one-sided Cauchy distribution (C6) for varying the positive scaling parameter σ from $\bar{D}(z = 1.0)/10$ to $\bar{D}(z = 1.0)/1000$ as indicated. From left to right, we present the pure local contributions, sum of pure nonlocal contributions and crosstalk between local and nonlocal contributions, and total contributions, respectively. Black lines represent the multipoles without the halo contributions.

We note that if the distribution, $f(\mathcal{D}_{\rm host})$, follows Gaussian statistics, this convolution induces an exponential suppression of Fourier modes along the line-of-sight direction (see, e.g., Ref. [70]).

Second, we consider the nonlocal contributions. As we formulate the correlation function of the nonlocal terms with taking the plane-parallel limit and Limber approximation, the Fourier modes parallel to the line-of-sight direction do not contribute to the resultant correlation function. Furthermore, in the plane-parallel limit, we have $\chi_1 = \chi_2 \simeq \chi$, suggesting that we simply replace the comoving distance χ in the expression of the correlation function by $\chi + \Delta\chi$. Schematically, denoting the original expression of the correlation function by $\xi(\chi)$, which ignores the host galaxy contributions, it is modified by

$$\tilde{\xi}(\chi) = \int_0^\infty \mathrm{d}\mathcal{D}_{\rm host}\xi(\chi + \Delta\chi(z, D_{\rm host}))f(\mathcal{D}_{\rm host}). \tag{C5}$$

This is the case for the pure nonlocal contribution and crosstalk between local and nonlocal contributions. We note that this argument is valid for the analytical expression in the plane-parallel limit and Limber approximation.

With Eqs. (C4) and (C5), we demonstrate the host galaxy contributions. To do so, we need to assume the explicit form of the distribution function $f(\mathcal{D}_{\rm host})$. Although its functional form should be refined by simulations or observations, we simply assume that $f(\mathcal{D}_{\rm host})$ obeys the one-sided Cauchy distribution with a positive scale parameter σ,

$$f(\mathcal{D}_{\rm host}) = \frac{2}{\pi\sigma}\frac{1}{1 + \mathcal{D}_{\rm host}^2/\sigma^2}, \tag{C6}$$

where we set a location parameter of the one-sided Cauchy distribution to zero, for simplicity, and hence, this distribution is only supported for $\mathcal{D}_{\rm host} > 0$.

We demonstrate the impact of the halo contribution to the correlation function. For the quantitative demonstration, we show the multipoles of FRBs for varying σ in Fig. 11. As we increase σ, the local terms are monotonically smeared but the nonlocal terms exhibit nonmonotonic behavior, because of the explicit χ dependence appearing in $\mathcal{A}(\chi)$ or in the lensing kernel $(\chi' - \chi)/\chi$. If the total signal is dominated by the nonlocal terms such as the even multipoles, the halo contribution would weakly change the observed signal. However, since the local terms induce a non-negligible contribution to the dipole moment, careful treatment of the halo contribution would be required. We note that the above discussion is based on crude modeling of the halo contribution. Hence, the halo contribution should be refined by hydrodynamic simulations to provide a more realistic forecast, in future work.

[1] D. R. Lorimer, M. Bailes, M. A. McLaughlin, D. J. Narkevic, and F. Crawford, A bright millisecond radio burst of extragalactic origin, Science **318**, 777 (2007).

[2] S. R. Kulkarni, Dispersion measure: Confusion, constants & clarity, arXiv:2007.02886.

[3] E. Petroff, E. D. Barr, A. Jameson, E. F. Keane, M. Bailes, M. Kramer, V. Morello, D. Tabbara, and W. van Straten, FRBCAT: The fast radio burst catalogue, Pub. Astron. Soc. Aust. **33**, e045 (2016).

[4] S. P. Tendulkar *et al.*, The host galaxy and redshift of the repeating fast radio burst FRB 121102, Astrophys. J. Lett. **834**, L7 (2017).

[5] S. Chatterjee *et al.*, A direct localization of a fast radio burst and its host, Nature (London) **541**, 58 (2017).

[6] J. P. Macquart, J. X. Prochaska, M. McQuinn, K. W. Bannister, S. Bhandari, C. K. Day, A. T. Deller, R. D. Ekers, C. W. James, L. Marnoch, S. Osłowski, C. Phillips, S. D. Ryder, D. R. Scott, R. M. Shannon, and N. Tejos, A census of baryons in the Universe from localized fast radio bursts, Nature (London) **581**, 391 (2020).

[7] M. Amiri *et al.* (CHIME/FRB Collaboration), The first CHIME/FRB fast radio burst catalog, Astrophys. J. Suppl. Ser. **257**, 59 (2021).

[8] E. Platts, A. Weltman, A. Walters, S. P. Tendulkar, J. E. B. Gordin, and S. Kandhai, A living theory catalogue for fast radio bursts, Phys. Rep. **821**, 1 (2019).

[9] J. M. Cordes and S. Chatterjee, Fast radio bursts: An extragalactic enigma, Annu. Rev. Astron. Astrophys. **57**, 417 (2019).

[10] E. Petroff, J. W. T. Hessels, and D. R. Lorimer, Fast radio bursts, Astron. Astrophys. Rev. **27**, 4 (2019).

[11] M. Caleb, C. Flynn, M. Bailes, E. D. Barr, T. Bateman, S. Bhandari, D. Campbell-Wilson, A. J. Green, R. W. Hunstead, A. Jameson, F. Jankowski, E. F. Keane, V. Ravi, W. van Straten, and V. V. Krishnan, Fast radio transient searches with UTMOST at 843 MHz, Mon. Not. R. Astron. Soc. **458**, 718 (2016).

[12] L. B. Newburgh *et al.*, HIRAX: A probe of dark energy and radio transients, in *Ground-based and Airborne Telescopes VI*, Society of Photo-Optical Instrumentation Engineers (SPIE) Conference Series Vol. 9906, edited by H. J. Hall, R. Gilmozzi, and H. K. Marshall (2016), p. 99065X, 10.1117/12.2234286.

[13] A. Rane, D. R. Lorimer, S. D. Bates, N. McMann, M. A. McLaughlin, and K. Rajwade, A search for rotating radio transients and fast radio bursts in the Parkes high-latitude pulsar survey, Mon. Not. R. Astron. Soc. **455**, 2207 (2016).

[14] L. Connor, H.-H. Lin, K. Masui, N. Oppermann, U.-L. Pen, J. B. Peterson, A. Roman, and J. Sievers, Constraints on the FRB rate at 700–900 MHz, Mon. Not. R. Astron. Soc. **460**, 1054 (2016).

[15] T. Hashimoto, T. Goto, A. Y. L. On, T.-Y. Lu, D. J. D. Santos, S. C. C. Ho, T.-W. Wang, S. J. Kim, and T. Y. Y. Hsiao, Fast radio bursts to be detected with the Square Kilometre Array, Mon. Not. R. Astron. Soc. **497**, 4107 (2020).

[16] W. Deng and B. Zhang, Cosmological implications of fast radio burst/gamma-ray burst associations, Astrophys. J. Lett. **783**, L35 (2014).

[17] A. Fialkov and A. Loeb, Constraining the CMB optical depth through the dispersion measure of cosmological radio transients, J. Cosmol. Astropart. Phys. 05 (2016) 004.

[18] M. S. Madhavacheril, N. Battaglia, K. M. Smith, and J. L. Sievers, Cosmology with kSZ: Breaking the optical depth degeneracy with Fast Radio Bursts, Phys. Rev. D **100**, 103532 (2019).

[19] M. Caleb, C. Flynn, and B. W. Stappers, Constraining the era of helium reionization using fast radio bursts, Mon. Not. R. Astron. Soc. **485**, 2281 (2019).

[20] P. Beniamini, P. Kumar, X. Ma, and E. Quataert, Exploring the epoch of hydrogen reionization using FRBs, Mon. Not. R. Astron. Soc. **502**, 5134 (2021).

[21] M. Bhattacharya, P. Kumar, and E. V. Linder, Fast radio burst dispersion measure distribution as a probe of helium reionization, Phys. Rev. D **103**, 103526 (2021).

[22] M. Pagano and H. Fronenberg, Constraining the epoch of reionization with highly dispersed fast radio bursts, Mon. Not. R. Astron. Soc. **505**, 2195 (2021).

[23] S. Heimersheim, N. S. Sartorio, A. Fialkov, and D. R. Lorimer, What it takes to measure reionization with fast radio bursts, Astrophys. J. **933**, 57 (2022).

[24] Z. Li, H. Gao, J.-J. Wei, Y.-P. Yang, B. Zhang, and Z.-H. Zhu, Cosmology-independent estimate of the fraction of baryon mass in the IGM from fast radio burst observations, Astrophys. J. **876**, 146 (2019).

[25] J.-J. Wei, Z. Li, H. Gao, and X.-F. Wu, Constraining the evolution of the baryon fraction in the IGM with FRB and H (z) data, J. Cosmol. Astropart. Phys. 09 (2019) 039.

[26] Z. Li, H. Gao, J. J. Wei, Y. P. Yang, B. Zhang, and Z. H. Zhu, Cosmology-insensitive estimate of IGM baryon mass fraction from five localized fast radio bursts, Mon. Not. R. Astron. Soc. **496**, L28 (2020).

[27] T. Lemos, R. S. Gonçalves, J. C. Carvalho, and J. S. Alcaniz, Cosmological model-independent constraints on the baryon fraction in the IGM from fast radio bursts and supernovae data, Eur. Phys. J. C **83**, 138 (2023).

[28] A. Nicola, F. Villaescusa-Navarro, D. N. Spergel, J. Dunkley, D. Anglés-Alcázar, R. Davé, S. Genel, L. Hernquist, D. Nagai, R. S. Somerville, and B. D. Wandelt, Breaking baryon-cosmology degeneracy with the electron density power spectrum, J. Cosmol. Astropart. Phys. 04 (2022) 046.

[29] A. Theis, S. Hagstotz, R. Reischke, and J. Weller, Galaxy dispersion measured by Fast Radio Bursts as a probe of baryonic feedback models, arXiv:2403.08611.

[30] K. Ioka, The cosmic dispersion measure from gamma-ray burst afterglows: Probing the reionization history and the burst environment, Astrophys. J. Lett. **598**, L79 (2003).

[31] S. Inoue, Probing the cosmic reionization history and local environment of gamma-ray bursts through radio dispersion, Mon. Not. R. Astron. Soc. **348**, 999 (2004).

[32] M. McQuinn, Locating the "missing" baryons with extragalactic dispersion measure estimates, Astrophys. J. Lett. **780**, L33 (2014).

[33] J. P. Macquart, E. Keane, K. Grainge, M. McQuinn, R. Fender, J. Hessels, A. Deller, R. Bhat, R. Breton, S. Chatterjee, C. Law, D. Lorimer, E. O. Ofek, M. Pietka, L. Spitler, B. Stappers, and C. Trott, Fast transients at cosmological distances with the SKA, in *Proceedings of the*

Advancing Astrophysics with the Square Kilometre Array (AASKA14) (2015), p. 55; arXiv:1501.07535.

[34] V. Ravi, Measuring the circumgalactic and intergalactic baryon contents with fast radio bursts, Astrophys. J. **872**, 88 (2019).

[35] B. Zhou, X. Li, T. Wang, Y.-Z. Fan, and D.-M. Wei, Fast radio bursts as a cosmic probe?, Phys. Rev. D **89**, 107303 (2014).

[36] P. Kumar and E. V. Linder, Use of fast radio burst dispersion measures as distance measures, Phys. Rev. D **100**, 083533 (2019).

[37] B. Liu, Z. Li, H. Gao, and Z.-H. Zhu, Prospects of strongly lensed repeating fast radio bursts: Complementary constraints on dark energy evolution, Phys. Rev. D **99**, 123517 (2019).

[38] Z.-W. Zhao, Z.-X. Li, J.-Z. Qi, H. Gao, J.-F. Zhang, and X. Zhang, Cosmological parameter estimation for dynamical dark energy models with future fast radio burst observations, Astrophys. J. **903**, 83 (2020).

[39] X.-W. Qiu, Z.-W. Zhao, L.-F. Wang, J.-F. Zhang, and X. Zhang, A forecast of using fast radio burst observations to constrain holographic dark energy, J. Cosmol. Astropart. Phys. 02 (2022) 006.

[40] Z.-W. Zhao, L.-F. Wang, J.-G. Zhang, J.-F. Zhang, and X. Zhang, Probing the interaction between dark energy and dark matter with future fast radio burst observations, J. Cosmol. Astropart. Phys. 04 (2023) 022.

[41] H. Gao, Z. Li, and B. Zhang, Fast radio burst/gamma-ray burst cosmography, Astrophys. J. **788**, 189 (2014).

[42] Y.-P. Yang and B. Zhang, Extracting host galaxy dispersion measure and constraining cosmological parameters using fast radio burst data, Astrophys. J. Lett. **830**, L31 (2016).

[43] A. Walters, A. Weltman, B. M. Gaensler, Y.-Z. Ma, and A. Witzemann, Future cosmological constraints from fast radio bursts, Astrophys. J. **856**, 65 (2018).

[44] M. Jaroszynski, Fast radio bursts and cosmological tests, Mon. Not. R. Astron. Soc. **484**, 1637 (2019).

[45] J.-G. Zhang, Z.-W. Zhao, Y. Li, J.-F. Zhang, D. Li, and X. Zhang, Cosmology with fast radio bursts in the era of SKA, Sci. China Phys. Mech. Astron. **66**, 120412 (2023).

[46] C. W. James, E. M. Ghosh, J. X. Prochaska, K. W. Bannister, S. Bhandari, C. K. Day, A. T. Deller, M. Glowacki, A. C. Gordon, K. E. Heintz, L. Marnoch, S. D. Ryder, D. R. Scott, R. M. Shannon, and N. Tejos, A measurement of Hubble's constant using fast radio bursts, Mon. Not. R. Astron. Soc. **516**, 4862 (2022).

[47] Q. Wu, G.-Q. Zhang, and F.-Y. Wang, An 8 per cent determination of the Hubble constant from localized fast radio bursts, Mon. Not. R. Astron. Soc. **515**, L1 (2022).

[48] S. Hagstotz, R. Reischke, and R. Lilow, A new measurement of the Hubble constant using fast radio bursts, Mon. Not. R. Astron. Soc. **511**, 662 (2022).

[49] Z.-W. Zhao, J.-G. Zhang, Y. Li, J.-M. Zou, J.-F. Zhang, and X. Zhang, First statistical measurement of the Hubble constant using unlocalized fast radio bursts, arXiv:2212.13433.

[50] Y. Liu, H. Yu, and P. Wu, Cosmological-model-independent Determination of Hubble constant from fast radio bursts and Hubble parameter measurements, Astrophys. J. Lett. **946**, L49 (2023).

[51] J. Gao, Z. Zhou, M. Du, R. Zou, J. Hu, and L. Xu, A measurement of Hubble constant using cosmographic approach combining fast radio bursts and supernovae, Mon. Not. R. Astron. Soc. **527**, 7861 (2024).

[52] J.-J. Wei, H. Gao, X.-F. Wu, and P. Mészáros, Testing Einstein's equivalence principle with fast radio bursts, Phys. Rev. Lett. **115**, 261101 (2015).

[53] A. Nusser, On testing the equivalence principle with extragalactic bursts, Astrophys. J. Lett. **821**, L2 (2016).

[54] S. J. Tingay and D. L. Kaplan, Limits on Einstein's equivalence principle from the first localized fast radio burst FRB 150418, Astrophys. J. Lett. **820**, L31 (2016).

[55] R. Reischke, S. Hagstotz, and R. Lilow, Consistent equivalence principle tests with fast radio bursts, Mon. Not. R. Astron. Soc. **512**, 285 (2022).

[56] R. Reischke, S. Hagstotz, and R. Lilow, Probing primordial non-Gaussianity with fast radio bursts, Phys. Rev. D **103**, 023517 (2021).

[57] K. W. Masui and K. Sigurdson, Dispersion distance and the matter distribution of the universe in dispersion space, Phys. Rev. Lett. **115**, 121301 (2015).

[58] M. Rafiei-Ravandi, K. M. Smith, and K. W. Masui, Characterizing fast radio bursts through statistical cross-correlations, Phys. Rev. D **102**, 023528 (2020).

[59] D. Alonso, Linear anisotropies in dispersion-measure-based cosmological observables, Phys. Rev. D **103**, 123544 (2021).

[60] H. Xiao, L. Dai, and M. McQuinn, Detecting dark matter substructures on small scales with fast radio bursts, Phys. Rev. D **110**, 023516 (2024).

[61] M. Sasaki, The magnitude-redshift relation in a perturbed Friedmann universe, Mon. Not. R. Astron. Soc. **228**, 653 (1987).

[62] T. Matsubara, The gravitational lensing in redshift-space correlation functions of galaxies and quasars, Astrophys. J. Lett. **537**, L77 (2000).

[63] A. Challinor and A. Lewis, Linear power spectrum of observed source number counts, Phys. Rev. D **84**, 043516 (2011).

[64] C. Bonvin and R. Durrer, What galaxy surveys really measure, Phys. Rev. D **84**, 063505 (2011).

[65] P. McDonald, Gravitational redshift and other redshift-space distortions of the imaginary part of the power spectrum, J. Cosmol. Astropart. Phys. 11 (2009) 026.

[66] R. A. C. Croft, Gravitational redshifts from large-scale structure, Mon. Not. R. Astron. Soc. **434**, 3008 (2013).

[67] J. Yoo, N. Hamaus, U. Seljak, and M. Zaldarriaga, Going beyond the Kaiser redshift-space distortion formula: A full general relativistic account of the effects and their detectability in galaxy clustering, Phys. Rev. D **86**, 063514 (2012).

[68] V. Tansella, C. Bonvin, R. Durrer, B. Ghosh, and E. Sellentin, The full-sky relativistic correlation function and power spectrum of galaxy number counts. Part I: Theoretical aspects, J. Cosmol. Astropart. Phys. 03 (2018) 019.

[69] C. Bonvin, L. Hui, and E. Gaztañaga, Asymmetric galaxy correlation functions, Phys. Rev. D **89**, 083535 (2014).

[70] T. Namikawa, Analyzing clustering of astrophysical gravitational-wave sources: Luminosity-distance space distortions, J. Cosmol. Astropart. Phys. 01 (2021) 036.

[71] S. Alam, H. Zhu, R. A. C. Croft, S. Ho, E. Giusarma, and D. P. Schneider, Relativistic distortions in the large-scale clustering of SDSS-III BOSS CMASS galaxies, Mon. Not. R. Astron. Soc. **470**, 2822 (2017).
[72] D. N. Limber, The analysis of counts of the extragalactic nebulae in terms of a fluctuating density field, Astrophys. J. **117**, 134 (1953).
[73] N. Afshordi, Y.-S. Loh, and M. A. Strauss, Cross-correlation of the cosmic microwave background with the 2 MASS galaxy survey: Signatures of dark energy, hot gas, and point sources, Phys. Rev. D **69**, 083524 (2004).
[74] L. Hui, E. Gaztañaga, and M. Loverde, Anisotropic magnification distortion of the 3D galaxy correlation. I. Real space, Phys. Rev. D **76**, 103502 (2007).
[75] V. Tansella, G. Jelic-Cizmek, C. Bonvin, and R. Durrer, COFFE: A code for the full-sky relativistic galaxy correlation function, J. Cosmol. Astropart. Phys. 10 (2018) 032.
[76] G. Jelic-Cizmek, The flat-sky approximation to galaxy number counts—redshift space correlation function, J. Cosmol. Astropart. Phys. 07 (2021) 045.
[77] J. Yoo, Relativistic effect in galaxy clustering, Classical Quantum Gravity **31**, 234001 (2014).
[78] E. Gaztanaga, C. Bonvin, and L. Hui, Measurement of the dipole in the cross-correlation function of galaxies, J. Cosmol. Astropart. Phys. 01 (2017) 032.
[79] M.-A. Breton, Y. Rasera, A. Taruya, O. Lacombe, and S. Saga, Imprints of relativistic effects on the asymmetry of the halo cross-correlation function: From linear to non-linear scales, Mon. Not. R. Astron. Soc. **483**, 2671 (2019).
[80] F. Beutler and E. Di Dio, Modeling relativistic contributions to the halo power spectrum dipole, J. Cosmol. Astropart. Phys. 07 (2020) 048.
[81] S. Saga, A. Taruya, M.-A. Breton, and Y. Rasera, Modelling the asymmetry of the halo cross-correlation function with relativistic effects at quasi-linear scales, Mon. Not. R. Astron. Soc. **498**, 981 (2020).
[82] S. Saga, A. Taruya, Y. Rasera, and M.-A. Breton, Detectability of the gravitational redshift effect from the asymmetric galaxy clustering, Mon. Not. R. Astron. Soc. **511**, 2732 (2022).
[83] S. Saga, A. Taruya, Y. Rasera, and M.-A. Breton, Cosmological test of local position invariance from the asymmetric galaxy clustering, Mon. Not. R. Astron. Soc. **524**, 4472 (2023).
[84] P. Bull, Extending cosmological tests of general relativity with the square kilometre array, Astrophys. J. **817**, 26 (2016).
[85] T. Pyne and M. Birkinshaw, The luminosity distance in perturbed FLRW space-times, Mon. Not. R. Astron. Soc. **348**, 581 (2004).
[86] J. Yoo, A. L. Fitzpatrick, and M. Zaldarriaga, New perspective on galaxy clustering as a cosmological probe: General relativistic effects, Phys. Rev. D **80**, 083514 (2009).
[87] J. Yoo, General relativistic description of the observed galaxy power spectrum: Do we understand what we measure?, Phys. Rev. D **82**, 083508 (2010).
[88] F. Lepori, E. Di Dio, E. Villa, and M. Viel, Optimal galaxy survey for detecting the dipole in the cross-correlation with 21 cm intensity mapping, J. Cosmol. Astropart. Phys. 05 (2018) 043.
[89] N. Kaiser, Clustering in real space and in redshift space, Mon. Not. R. Astron. Soc. **227**, 1 (1987).
[90] A. J. S. Hamilton, Measuring Omega and the real correlation function from the redshift correlation function, Astrophys. J. Lett. **385**, L5 (1992).
[91] K. Yamamoto, Optimal weighting scheme in redshift-space power spectrum analysis and a prospect for measuring the cosmic equation of state, Astrophys. J. **595**, 577 (2003).
[92] K. Yamamoto, M. Nakamichi, A. Kamino, B. A. Bassett, and H. Nishioka, A measurement of the quadrupole power spectrum in the clustering of the 2dF QSO survey, Publ. Astron. Soc. Jpn. **58**, 93 (2006).
[93] A. Taruya, T. Nishimichi, and S. Saito, Baryon acoustic oscillations in 2D: Modeling redshift-space power spectrum from perturbation theory, Phys. Rev. D **82**, 063522 (2010).
[94] A. Hall and C. Bonvin, Measuring cosmic velocities with 21 cm intensity mapping and galaxy redshift survey cross-correlation dipoles, Phys. Rev. D **95**, 043530 (2017).
[95] M. Vogelsberger, S. Genel, V. Springel, P. Torrey, D. Sijacki, D. Xu, G. Snyder, D. Nelson, and L. Hernquist, Introducing the illustris project: Simulating the coevolution of dark and visible matter in the Universe, Mon. Not. R. Astron. Soc. **444**, 1518 (2014).
[96] R. Takahashi, K. Ioka, A. Mori, and K. Funahashi, Statistical modelling of the cosmological dispersion measure, Mon. Not. R. Astron. Soc. **502**, 2615 (2021).
[97] J. Lesgourgues, The cosmic linear anisotropy solving system (CLASS) I: Overview, arXiv:1104.2932.
[98] B. Audren and J. Lesgourgues, Non-linear matter power spectrum from time renormalisation group: Efficient computation and comparison with one-loop, J. Cosmol. Astropart. Phys. 10 (2011) 037.